

Article

Not peer-reviewed version

Temperature Relaxation in Glass-Forming Materials under Local Fast Laser Excitations during Laser-Induced Microstructuring

[A. Minakov](#) and [C. Schick](#)*

Posted Date: 11 January 2024

doi: 10.20944/preprints202401.0948.v1

Keywords: glasses; dynamic heat capacity; nonequilibrium heat transfer; laser-induced microstructuring; femtosecond laser processing; optical storage



Preprints.org is a free multidiscipline platform providing preprint service that is dedicated to making early versions of research outputs permanently available and citable. Preprints posted at Preprints.org appear in Web of Science, Crossref, Google Scholar, Scilit, Europe PMC.

Copyright: This is an open access article distributed under the Creative Commons Attribution License which permits unrestricted use, distribution, and reproduction in any medium, provided the original work is properly cited.

Article

Temperature Relaxation in Glass-Forming Materials under Local Fast Laser Excitations during Laser-Induced Microstructuring

Minakov ¹ and C. Schick ^{2,*}

Prokhorov General Physics Institute of the Russian Academy of Sciences. Vavilov Str. 38, 119991 Moscow, Russia; minakov@nsc.gpi.ru

University of Rostock, Institute of Physics and Competence Centre CALOR. Albert-Einstein-Str. 23-24, 18051 Rostock, Germany; christoph.schick@uni-rostock.de

* Correspondence: christoph.schick@uni-rostock.de; Tel.: +49 381 498 6880

Featured Application: The obtained knowledge can be useful for understanding and optimizing various technologies with glass-forming materials under local fast laser excitations.

Abstract: The ability to control the temperature distribution $T(t, r)$ and the rate of temperature change $\mathcal{R}(t, r)$ inside glasses is important for their microstructuring. The lattice temperature is considered at time t , exceeding the electron-phonon thermalization time, and at a distance r from the center of the model spherical heating zone. In order to describe thermal excitations, the heat capacity of glasses must be considered as a function of time due to its long-term relaxation. A method for analytical calculation of $T(t, r)$ and $\mathcal{R}(t, r)$ for glasses with dynamic heat capacity $c_{dyn}(t)$ is proposed. It is shown that during laser microstructuring the local cooling rate $-\mathcal{R}(t, r)$ significantly depends on the time dispersion of $c_{dyn}(t)$. It has been established that at the periphery of the model heating zone of the laser beam focus, the local cooling rate can reach more than 10^{11} K/s. Strong cooling rate gradients were found at the periphery of the heating zone, affecting the microstructure of the material. This effect is significantly enhanced by the time dispersion of $c_{dyn}(t)$. The effect associated with this time dispersion is significant even well above the glass transition temperature T_g , since even short relaxation times of the dynamic heat capacity $c_{dyn}(t)$ are significant.

Keywords: glasses; dynamic heat capacity; nonequilibrium heat transfer; laser-induced microstructuring; femtosecond laser processing; optical storage

1. Introduction

Glass-forming materials are often used to create optical elements and components for optical integrated circuits. In the last two decades, the technology of femtosecond laser microfabrication of various optical structures inside glass-forming materials has been intensively developed. Due to the extremely high peak intensities at the focus of femtosecond laser pulses, nonlinear processes such as multiphoton absorption can lead to significant energy absorption even within transparent materials such as glass. Thus, femtosecond laser-induced microstructuring of glass-forming materials opens up wide possibilities for various applications. Laser radiation can cause irreversible local phenomena at the beam focus, such as phase transitions [1], the formation of bubbles or microfluidic channels [2–5], changes in chemical composition or refractive index [6,7], for example, diffusion and aggregation of silver ions [6] or photo-oxidation [7]. Spatially selective laser-induced crystallization or structure changes of glasses allows direct recording of channel waveguides [1,8–14]. In fact, laser-written waveguides (with improved mode structure of guided light) can be fabricated by local laser heating inside a glass matrix [8,9]. Thus, optical integrated circuits can be fabricated using a laser beam that induces local structural changes in a glass [15–18]. Photopolymerization and photodamage by highly focused laser pulses can be used in microchemistry and stereolithography [6,19]. Moreover, femtosecond laser structuring of glass-forming materials can be used for optical long-term storage of information [3,20–30], photonics [31], fabrication of phase gratings [32], nano-gratings [33], and

quantum dots that can be used in various devices [34–36]. Notably, optical storage based on glass-forming materials has the potential to replace magnetic storage in the quest to provide high-speed, high-capacity, low-power, low-cost, highly secure, and long-term data storage [25–30]. However, for the development of these technologies, theoretical models of thermal processes occurring during spatially selective laser-induced structuring of glass-forming materials are required. For example, understanding the dynamics of the laser crystallization process of amorphous Ge films is important for transistor technology, photovoltaic devices, particle detectors, and photodetectors [37]. In fact, the laser crystallization method makes it possible to control the local temperature inside the material and avoid random nucleation [37]. The ability to form and control the dynamics of changes in the temperature distribution $T(t, r)$ inside the material is very important for the opportunity to control the morphology of the laser-written structure inside the glass matrix [22,33,38]. Thus, a deep understanding of the thermal processes inside glass-forming materials under fast laser thermal perturbations is required. In this paper, we focus on local temperature changes, especially the local cooling rate $-\mathcal{R}(t, r)$ in the focal region during laser-writing processes in a glass matrix (where $\mathcal{R}(t, r)$ is the rate of temperature change).

Femtosecond laser-induced microstructuring is a promising tool because the structures induced by femtosecond laser pulses can be even smaller than the optical diffraction limit of the beam focusing, since multiphoton absorption is most effective in the central part of the beam focus. Typically, in laser-induced microstructuring, the laser pulse duration τ_{laser} is of the order of 100 fs and the radiation wavelength is about 1 μm . When a transparent material is irradiated with a powerful femtosecond laser pulse focused into a micro-sized focusing zone, multiphoton absorption of the laser radiation energy by electrons of the irradiated material occurs. The energy of the electrons in the laser focus increases sharply during τ_{laser} due to electron-photon interaction. The electrons then transfer their energy to the lattice through electron-phonon interaction. The thermalization process takes approximately tens or hundreds of picoseconds [6,10,39,40]. Consequently, the duration of heating pulses τ_p that heat the material can be on the order of tens to hundreds of picoseconds. Thus, the material can be locally heated above the glass transition temperature T_g and melting temperature T_m . Heat then spreads through the material and the hot focal zone is rapidly cooled below T_g .

In this article, we will consider laser pulses of moderate energy E_p (in the range 10 – 100 nJ), sufficient to locally heat the material well above the glass transition temperature T_g , but not sufficient to destroy the material with the formation of voids. Thus, the intensity of the laser pulses considered in this article is below the material damage threshold, which, for example, for silica glass is about 10^{16} W/cm² [41]. We focus on micrometer-scale local thermal perturbations caused by laser pulses near or below the threshold ionization intensity of a material. The threshold ionization intensity of most transparent solids ranges from 10^{13} to 10^{14} W/cm² for light with a wavelength of about 1 μm [42,43]. For example, the threshold intensity in silica glass and similar glass-forming materials is about 10^{13} W/cm² for light pulses with a wavelength of about 1 μm and a duration of 100 fs [42].

Thus, we will consider thermal processes in dielectric glasses below the threshold intensity of ionization of the material and in the time interval after electron-phonon thermalization, when there is no electron-hole plasma. Thus, we are interested in changes in lattice temperature on a time scale outside the time interval when a multi-temperature model is usually considered [12–14]. In fact, we are interested in changes in lattice temperature that affect the structure of the material at moderate laser pulse energies and time t exceeding the electron-phonon thermalization time.

The initial structure of glass-forming materials is not completely restored after the rapid heating-cooling cycle, which leads to a change in the local properties of the material in rapidly cooled areas. The local structure, specific volume, density, Rayleigh scattering loss and refractive index of glass-forming materials significantly depend on the local cooling rate [19,44,45], see Figure 1.

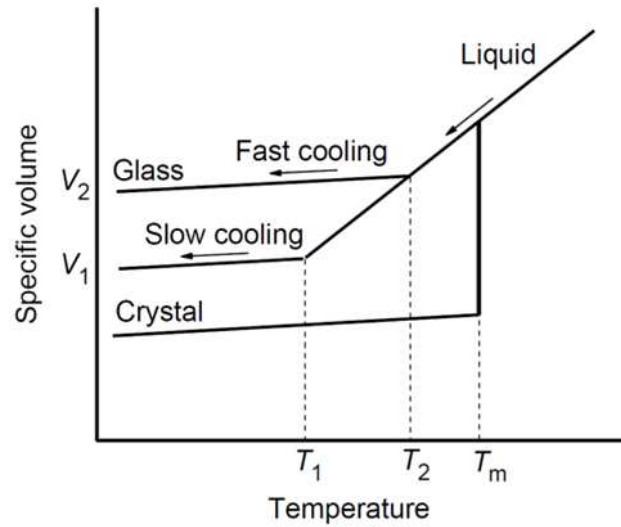


Figure 1. Schematic diagram of the specific volume V as a function of temperature T for glass-forming materials at different cooling rates $-\mathcal{R}_1$ and $-\mathcal{R}_2$. Liquid structures freeze to a glassy state with $V_2(\mathcal{R}_2) > V_1(\mathcal{R}_1)$ at $|\mathcal{R}_2| > |\mathcal{R}_1|$.

Thus, we focus on the dynamics of the temperature distribution $T(t, r)$ and study the local cooling rate $-\mathcal{R}(t, r)$ near the focal region during laser-induced microstructuring. Measurements of the temperature distribution at the focus of the laser beam can be carried out using micro-Raman spectroscopy [46–48]. However, the time resolution of Raman spectroscopy (with a measuring pulse duration of about 10 ns and a repetition rate of 1 kHz) is not sufficient to detect ultrafast changes in the local temperature $T(t, r)$. We found that the local cooling rate $-\mathcal{R}(t, r)$ after the end of the heating pulse can reach more than 10^{11} K/s in a thin layer around the focus of the laser beam. In fact, to resolve such ultrafast temperature changes at the periphery of the hot focal zone requires a temporal and spatial resolution of at least about 0.1 ns and 10 nm, respectively, since the cooling rate $-\mathcal{R}(t, r)$ reaches about 600 GK/s in a narrow layer around the hot zone at the laser focus (see below). Thus, the maximum change in the glass structure occurs at the periphery of the focal region (where the material undergoes ultrafast quenching). In fact, laser microstructuring of glasses makes it possible to form micron-sized domains that are close to spherical or ring-shaped, with a modified glass structure at the periphery of the domains [19,34,36,40,46,49–53]. For example, local modification of silver-doped phosphate glasses with the laser pulse energies E_p in the range of 10 – 100 nJ led to the formation of micron-sized ring-shaped domains due to the aggregation of silver nanoclusters at the periphery of the domains [49]. Laser pulse energy E_p and pulse repetition rate play an important role in the microstructuring of glass-forming materials. In fact, laser pulses with a sufficient repetition rate can provide cumulative heating near the focus of the laser beam. In this article we will focus on the effect of single laser pulses (the effect of repetition rate will be discussed in a separate article).

The temperature change associated with the heating pulse is of the order of $\Delta T = E_p / C_{loc}$, where $C_{loc} = \rho c_p V_0$ and V_0 are the heat capacity and volume of the heating zone; ρ and c_p are the density and specific heat capacity of the material. The thermal effect caused by elastic deformations is negligible compared to ΔT , at least at moderate E_p , say in the range of 10 – 100 nJ for a focal region of about 1 μm radius. Indeed, the thermoelastic pressure in the hot zone is less than the maximum pressure response $p_{max} = K_B \alpha_V \Delta T$ to the temperature change ΔT at constant volume, where K_B and α_V are the bulk modulus and the volumetric thermal expansion coefficient. However, the volume of the hot zone is not rigidly fixed by the material surrounding this zone. In fact, a pressure wave is created around the hot zone [54,55]. In this case, the thermoelastic pressure is even less than p_{max} . Thus, the elastic energy associated with the thermoelastic pressure in the hot zone of volume V_0 is less than $E_{TE} = \frac{1}{2} K_B (\alpha_V \Delta T)^2 V_0$. Therefore, the relative effect associated with thermoelastic deformations does not exceed $E_{TE} / E_p = \frac{1}{2} K_B (\alpha_V)^2 \Delta T / \rho c_p$. For example, for sodium-lime-silicate

glasses with the composition $\text{Na}_2\text{O}\cdot 2\text{CaO}\cdot 3\text{SiO}_2$, E_{TE}/E_p is about 1% at $\Delta T = 2000$ K, $K_B = 55$ GPa, $\rho = 2.8$ g/cm³, $c_p = 1.14$ J/gK, $\alpha_V = 3\alpha$, and linear thermal expansion $\alpha = 7.7\cdot 10^{-6}$ 1/K [56–60]. This ratio is even lower for borosilicate glasses with a low coefficient of thermal expansion [61]. For example, for borosilicate glasses such as Pyrex, the E_{TE}/E_p ratio is about 0.1% at $\Delta T = 2000$ K, $K_B = 33$ GPa, $\rho = 2.23$ g/cm³, $c_p = 1.1$ J/gK, and $\alpha = 3.3\cdot 10^{-6}$ 1/K [61–64]. However, E_{TE} becomes comparable with E_p at laser pulse energies approximately 2 orders of magnitude higher than those considered in this work. We are interested in local temperature changes in a micron-sized hot zone at $t > \tau_p$, when the pressure waves created around the hot zone are already at a distance of more than 1–2 μm from the hot zone. However, at the same time, the front of the temperature change extends only about ten nanometers from the periphery of the hot zone. Thus, we consider the change in local temperature after the local pressure in the hot zone has almost stabilized. For example, in silicate glasses at $t = 0.5$ ns, the distance tV_L is about 3 μm at the longitudinal speed of sound $V_L \approx 6\cdot 10^3$ m/s [59], and $\sqrt{tD_0} \approx 10$ nm at the thermal diffusion coefficient D_0 of about $3\cdot 10^{-7}$ m²/s [57,63,65].

It is noteworthy that an important property of glass-forming materials is the long-term relaxation of the specific heat capacity with rapid changes in temperature. Thus, the heat capacity of glass-forming materials must be considered as a function of time $c_{dyn}(t)$ [66–68]. In fact, if a glass-forming material is heated to a liquid state with heat capacity c_L from a solid glassy state with heat capacity c_S , then the heat capacity of the material does not change immediately with the change in temperature, but slowly relaxes from c_S to c_L , see below. Long-term relaxation of the dynamic heat capacity $c_{dyn}(t)$ of glasses is due to the slow exchange of energy between different degrees of freedom in glasses. Thus, the thermal response of glass-forming materials to a thermal perturbation at time t depends on the temperature at earlier times. The effect of long-term relaxation of dynamic heat capacity significantly affects the dynamics of local temperature changes $T(t, r)$ [69,70]. In turn, the rate of change in local temperature $T(t, r)$ can significantly affect the micro-structuring of glass-forming materials [19,38,44,45,71]. An experimental study of the dynamics of the temperature distribution $T(t, r)$ inside a glass matrix under the action of fast laser thermal perturbations is very difficult. Therefore, it is necessary to develop theoretical models of thermal processes occurring during laser-induced structuring of glasses. In this paper, we will focus on modeling such thermal processes, taking into account the relaxation effect of the dynamic heat capacity $c_{dyn}(t)$. The dynamic behavior of glass-forming materials under fast local thermal perturbations can be described using the integro-differential heat equation with “memory” [69,70]. This equation has an analytical solution, at least in spherical, cylindrical and planar geometries [69,70,72]. This work aims to determine the dynamics of local temperature changes, especially the local rate of the temperature change $\mathcal{R}(t, r)$, associated with laser-induced thermal excitations during laser processing of glasses. An analytical method for determining $T(t, r)$ and $\mathcal{R}(t, r)$ has been developed. The knowledge obtained can be useful for various technologies related to laser-induced microstructuring.

In the first part of the article, the heat equation with dynamic heat capacity $c_{dyn}(t)$ is considered. An analysis of the dynamic heat capacity $c_{dyn}(t)$ of glass-forming materials has been conducted and an analytical solution of the heat equation with dynamic heat capacity for a spherically symmetric problem has been constructed. Then, the temperature distribution $T(t, r)$ is calculated for glasses with dynamic heat capacity $c_{dyn}(t)$ under local fast laser excitations. Examples with borosilicate and sodium-lime-silicate glasses are considered at different heating pulses and dynamic heat capacity parameters. Finally, the local distribution of the cooling rate $-\mathcal{R}(t, r)$ and its influence on the microstructuring processes of glasses is discussed.

2. Heat equation with dynamic heat capacity

Since the pioneering work of Birge and Nagel [66], the dynamic heat capacity $c_{dyn}(t)$ of glass-forming materials as a function of frequency (or time t) has been intensively studied. For such studies, heat capacity spectroscopy can be used [67,68]. The time dispersion of the dynamic heat capacity $c_{dyn}(t)$ can be described within the framework of linear response theory [73], similar to the time dispersion of the dielectric constant [74]. Then, heat transfer in the glass-forming material can

be described by an integro-differential heat equation [69,70]. In the case of spherical geometry and zero initial conditions, this heat equation can be represented in the following form [69,70]:

$$\frac{\partial}{\partial t} \int_0^t \rho c_{dyn}(t-\tau) T'(\tau, r) d\tau - \lambda \Delta T(t, r) = \Phi(t, r), \quad (1)$$

where $\Phi(t, r)$ is the volumetric heat flux density, $T'(t, r) = \frac{\partial}{\partial t} T(t, r)$, Δ – Laplacian, λ and ρ are the thermal conductivity and density of the material. Eq.(1) has an analytical solution for homogeneous boundary conditions, see below.

2.1. Dynamic heat capacity of glass-forming materials

The dynamic heat capacity $c_{dyn}(t)$ as a function of time can be represented as a continuous sum of exponential decays, since $c_{dyn}(t)$ is a monotonically relaxing function of time [69,70,75]:

$$c_{dyn}(t) = c_0 - (c_0 - c_{in}) \int_0^\infty H(\tau_0) \exp(-t/\tau_0) d\tau_0, \quad (2)$$

where c_{in} and c_0 are the initial and final (equilibrium) heat capacities: $c_{dyn}(t) \rightarrow c_{in}$ as $t \rightarrow 0$ and $c_{dyn}(t) \rightarrow c_0$ as $t \rightarrow \infty$. In fact, $c_{in} = c_s$ and $c_0 = c_L$ if the material is heated from a solid glassy state to a liquid one. The distribution function $H(\tau_0)$ of relaxation times τ_0 can be found using broadband heat capacity spectroscopy [68], for details see [69,70,72]. The dynamic heat capacity $c_{dyn}(t)$ is usually described by the Kohlrausch–Williams–Watts stretched exponent $\exp(-(t/\tau_K)^\beta)$ for $0 < \beta \leq 1$, where the Kohlrausch relaxation time τ_K and constant β characterize the relaxation time spectrum of the material [45,76,77]. In this case,

$$c_{dyn}(t) = c_0 [1 - \varepsilon_0 \exp(-(t/\tau_K)^\beta)], \quad (3)$$

where $\varepsilon_0 = (c_0 - c_{in})/c_0$. Usually, ε_0 is about 0.3 – 0.5 [68,78]. For example, if $\beta = 0.5$, then $H(\tau_0) = \frac{\exp(-\tau_0/4\tau_K)}{\sqrt{4\pi\tau_K\tau_0}}$ [76,77]. Thus, $c_{dyn}(t)$ can be approximately represented by Eq.(4) for a sufficiently large finite interval $[\tau_{min}, \tau_{max}]$:

$$c_{dyn}(t, \tau_K) \approx c_0 \left[1 - \varepsilon_0 \int_{\tau_{min}}^{\tau_{max}} \frac{\exp(-\tau_0/4\tau_K)}{\sqrt{4\pi\tau_K\tau_0}} \exp(-t/\tau_0) d\tau_0 \right], \quad (4)$$

where τ_K is a function of temperature. The function $\tau_K(T)$ can be obtained from the Vogel–Fulcher–Tammann–Hesse (VFTH) relation measured by broadband heat capacity spectroscopy [68]:

$$f_{max} = f_0 \exp[-B/(T - T_0)], \quad (5)$$

where f_{max} is the frequency corresponding to the maximum value of the temperature dependence of the imaginary part of the dynamic heat capacity $c_{dyn}(\omega)$ and $\omega = 2\pi f$ is the temperature modulation frequency; f_0 , B and T_0 are the VFTH parameters. In fact, $\tau_K \omega$ is about 1. More precisely, τ_K for different T can be obtained from the relation $\tau_K = \frac{0.737}{2\pi f_{max}}$ [69]. However, the shape of the distribution function $H(\tau_0)$ has insignificant effect on $T(t, r)$, since the effect due to the time dispersion of the dynamic heat capacity reaches saturation with increasing τ_0 , see below. Thus, it is sufficient to consider the dynamic heat capacity with the Debye relaxation law (see Eq.(6)) for sufficiently large τ_0 . Below we will show that this result practically coincides with the result obtained after averaging over the distribution function $H(\tau_0)$. In the case of the Debye relaxation law, $c_{dyn}(t)$ is equal to

$$c_{dyn}(t) = c_0 [1 - \varepsilon_0 \exp(-t/\tau_0)]. \quad (6)$$

In this case, the integro-differential heat equation Eq.(1) is transformed into Eq.(7), which can be solved analytically. After this, solutions for different τ_0 can be averaged using the distribution function $H(\tau_0)$.

2.2. Analytical solution of the heat equation with dynamic heat capacity

Let us consider the temperature distribution $T(t, r)$ after a single laser pulse in a micron-sized focal zone. A relatively small change in the thermal conductivity of the glass matrix around the hot focal zone does not affect the dynamics of the temperature distribution in the hot focal zone. In fact, for the glass-forming materials under consideration, λ varies insignificantly with temperature and is about $1 \text{ W/m}^2\text{K}$ over a wide temperature range [65,79,80]. Thus, it is assumed that the thermal conductivity λ of the glass matrix does not depend on temperature. However, the change in dynamic heat capacity $c_{dyn}(t)$ from c_S to c_L during heating is significant.

As a first step we consider the Debye relaxation law, see Eq.(6). Thus, for spherical geometry, from Eq.(1) we obtain Eq.(7):

$$\frac{\partial}{\partial t} T(t, r) - D_0 \Delta T(t, r) = \frac{\Phi(t, r)}{\rho c_0} + \varepsilon_0 \frac{\partial}{\partial t} \int_0^t \exp\left(-\frac{t-\tau}{\tau_0}\right) T'(t, r) d\tau, \quad (7)$$

where $D_0 = \lambda/\rho c_0$, and the spherically symmetric heat source $\Phi(t, r) = \Phi(r)F(t)$ is distributed in a spherical volume of radius r_0 . The decomposition of $\Phi(t, r)$ into the product $\Phi(r)F(t)$ is common for laser heating. Furthermore, after the end of the heating pulse, the temperature distribution $T(t, r)$ does not depend on the shape of $F(t)$, see below. In this article we are interested in the dynamics of the temperature distribution $T(t, r)$ after the heating pulse, when the shape of the heating pulse does not matter.

Consider Eq.(7) under the following initial conditions: $\Phi(t, r) = 0$ and $T(t, r) = T_{in}$ for $t \leq 0$, where T_{in} is the initial temperature in the glass matrix. Let $T(t, r)$ be a bounded function and $T(t, R_0) = T_{in}$ for $R_0 \gg r_0$. Since we are considering a single heating pulse, it does not matter how large the parameter R_0 is, as long as $R_0 \gg r_0$. Indeed, the temperature change is localized in a hot zone about a few micrometers in size, see below. The solution to this boundary value problem can be represented in the form of the following series (for details, see Appendix A):

$$T(t, r) = T_{in} + \sum_{n=1} \psi_n(t) \frac{\sin(\pi n r / R_0)}{r}, \quad (8)$$

where the functions $\psi_n(t)$ are determined by Eq.(9).

$$\psi_n'(t) + \frac{\psi_n(t)}{\tau_n} = \frac{\Phi_n F(t)}{\rho c_0} + \varepsilon_0 \frac{\partial}{\partial t} \int_0^t \exp\left(-\frac{t-\tau}{\tau_0}\right) \psi_n'(\tau) d\tau, \quad (9)$$

where $\Phi_n = \frac{2}{R_0} \int_0^{R_0} r \Phi(r) \sin(\pi n r / R_0) dr$ and $\tau_n^{-1} = D_0 (\pi n / R_0)^2$. Functions $\psi_n(t)$ satisfying Eq.(9) are presented in Appendix A. The spatial distribution $\Phi(r)$ of the heating power $\Phi(t, r)$ can be arbitrary. For example, we consider a heat source uniformly distributed in a volume of radius r_0 with volumetric density Φ_0 (in W/m^3), then

$$\Phi_n = 2R_0 \Phi_0 \frac{\sin(\pi n r_0 / R_0) - (\pi n r_0 / R_0) \cdot \cos(\pi n r_0 / R_0)}{(\pi n)^2}. \quad (10)$$

In fact, the distribution of the intensity of light radiation in the spot of a focused laser beam, depending on the distance r from the center of the spot, can have a Gaussian bell-shaped character, see Figure2. However, the intensity sufficient to induce nonlinear processes such as multiphoton absorption is located close to the center of the laser beam spot [5]. Thus, the model of a heat source uniformly distributed in a volume of radius r_0 with a sharp drop at the periphery is more realistic than the bell-shaped Gaussian distribution.

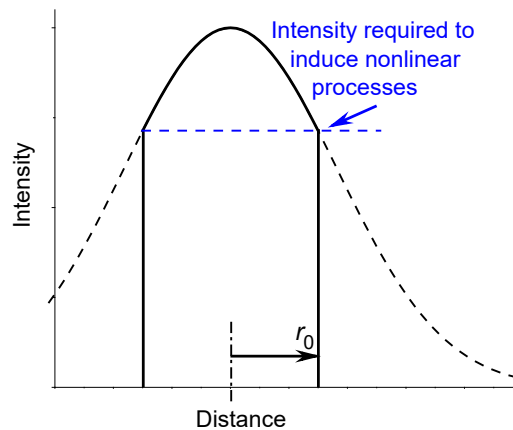


Figure 2. Schematic diagram of the distribution of the intensity of light radiation in a spot of a focused laser beam depending on the distance r from the center of the spot (dashed line) and the intensity distribution sufficient to induce nonlinear processes such as multiphoton absorption in a spot of radius r_0 (solid line).

The shape of the change in heating power over time can be bell-shaped or more complex. However, this shape is not significant for the temperature distribution $T(t, r)$ at $t > \tau_p$, see Figures 3 – 4. For model calculations, we will use a heating pulse of a half-sinusoidal shape, slightly different from the bell-shaped one. Thus, $F(t) = \sin(\pi t / \tau_p)$ for $0 \leq t \leq \tau_p$ and $F(t) = 0$ for $t > \tau_p$.

3. Temperature distribution $T(t, r)$ in glasses under local thermal perturbations

For example, let us consider the two most common types of silicate glasses: sodium-lime-silicate glasses ($\text{Na}_2\text{O}\cdot\text{CaO}\cdot\text{SiO}_2$), as the most widely used of all industrial glasses, known for their low cost and availability, and borosilicate glasses ($\text{B}_2\text{O}_3\cdot\text{SiO}_2$), which are widely used due to their low coefficient of thermal expansion and high resistance to chemical attack. Sodium-lime-silicate glass with the composition $\text{Na}_2\text{O}\cdot 2\text{CaO}\cdot 3\text{SiO}_2$ and borosilicate glass of the Pyrex type were chosen as model systems due to the availability of the necessary parameters [57,58,61–65]. The thermal parameters of these glasses are collected in Table 1.

Table 1. Thermal parameters of silicate glasses are used for model calculations.

Substance	Density in solid state ρ g/cm ³	Specific heat capacity in solid state c_p J/g·K	Volumetric heat capacity in solid state c_s J/m ³ K	Volumetric heat capacity in liquid state c_L J/m ³ K	Dynamic heat capacity parameter $\varepsilon_0 = (c_L - c_s) / c_L$	Thermal conductivity λ W/mK
Sodium-lime-silicate glass	2.8	1.14	$3.2 \cdot 10^6$	$4.4 \cdot 10^6$	0.273	1
Boro-silicate glass	2.23	1.1	$2.45 \cdot 10^6$	$3.8 \cdot 10^6$	0.355	1

3.1. Influence on $T(t, r)$ of the shape and duration of heating pulses

Thus, for model calculations, we use a heating pulse with a power density $\Phi_0 \sin(\pi t / \tau_p)$, acting during the time interval τ_p in a spherical region with a radius $r_0 = 1 \mu\text{m}$. Let us compare the results for heating pulses with $F(t)$, having half-sinusoidal and rectangular shapes, see Figures 3 and 4. Let the initial temperature $T_{in} = 300 \text{ K}$, $\tau_p = 300 \text{ ps}$, $E_p = 15 \text{ nJ}$, and the volume of the spherical heating zone $V_0 = \frac{4\pi}{3} r_0^3$. Thus, Φ_0 is equal to $\frac{\pi}{2} E_p / \tau_p V_0$ and $E_p / \tau_p V_0$ for half-sinusoidal and rectangular heating pulses, respectively. In this case, the energy of these pulses is the same and equal to E_p . The temperature distribution $T(t, r)$ can be calculated according to Eqs. (8) – (9) at various τ_0 .

For example, for sodium-lime-silicate glass (see Table 1), $T(t, r)$ at $\tau_0 = 0, 0.1 \mu\text{s}$, and $10 \mu\text{s}$ is represented in Figures 3 and 4. The temperature distribution $T(t, r)$ is calculated at $R_0 \gg r_0$ (for example, at $R_0 = 30 \mu\text{m}$). As follows from direct calculations, the result does not depend on R_0 , at least on the time scale $t < R_0^2/4D_0$, where $R_0^2/4D_0$ for the glasses under consideration is about 3–4 ms. Whereas we are interested in changes in the temperature distribution $T(t, r)$ on a time scale of microseconds and less, when the temperature changes are localized within a few micrometers, see Figure 3.

The influence of the time dispersion of the dynamic heat capacity $c_{dyn}(t)$ is significant, see Figures 3 and 4. The difference between equilibrium ($\tau_0 = 0$) and non-equilibrium ($\tau_0 \neq 0$) solutions $T(t, r)$ increases with the growth of τ_0 . The shape of the change in heating power over time is significant only during the time interval $(0, \tau_p)$, see Figure 4(a). However, this shape is not significant at $t > \tau_p$, see Figures 3 and 4(b).

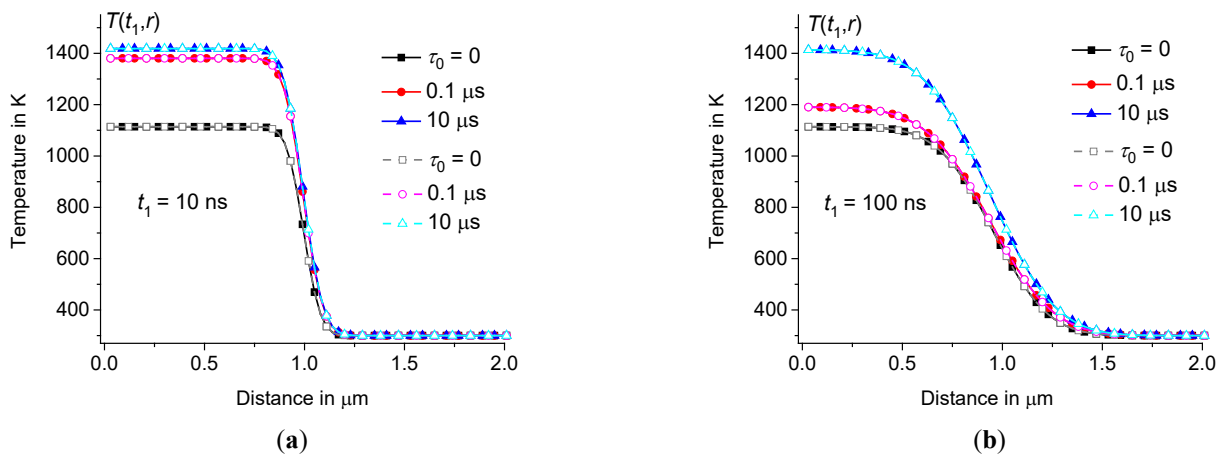


Figure 3. Temperature distribution $T(t_1, r)$ in the hot zone depending on the distance r at $t_1 = 10 \text{ ns}$ (a) and $t_1 = 100 \text{ ns}$ (b) for heating pulses of half-sinusoidal shape (filled symbols) and rectangular shape (open symbols) in sodium-lime-silicate glass at $r_0 = 1 \mu\text{m}$, $\tau_p = 300 \text{ ps}$, $E_p = 15 \text{ nJ}$, and $T_{in} = 300 \text{ K}$ ($\tau_0 = 0, 0.1 \mu\text{s}$, and $10 \mu\text{s}$ – squares, circles, and triangles, respectively).

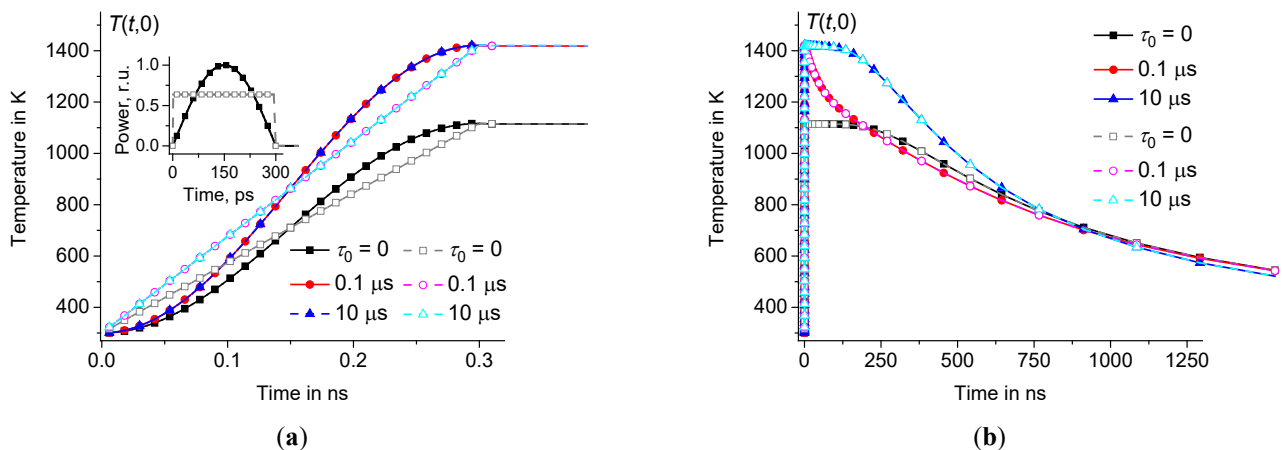


Figure 4. Time dependence of $T(t, 0)$ in the center of the hot zone during (a) and after (b) the heating pulses of half-sinusoidal shape (filled symbols) and rectangular shape (open symbols) at the same parameters as in Figure 3 ($\tau_0 = 0, 0.1 \mu\text{s}$, and $10 \mu\text{s}$ – squares, circles, and triangles, respectively). Inset (a) shows pulse power as a function of time.

The duration of the heating pulses is also not significant for the temperature distribution $T(t, r)$ at $t > \tau_p$, see Figure 5. For example, compare $T(t, r)$ for pulses τ with $\tau_p = 10 \text{ ps}$ and 300 ps and the

same parameters as in Figure3. The duration of heating pulses is significant only during the time interval $(0, \tau_p)$, see Figure5(a). However, this duration is not significant at $t > \tau_p$, see Figure5(b).

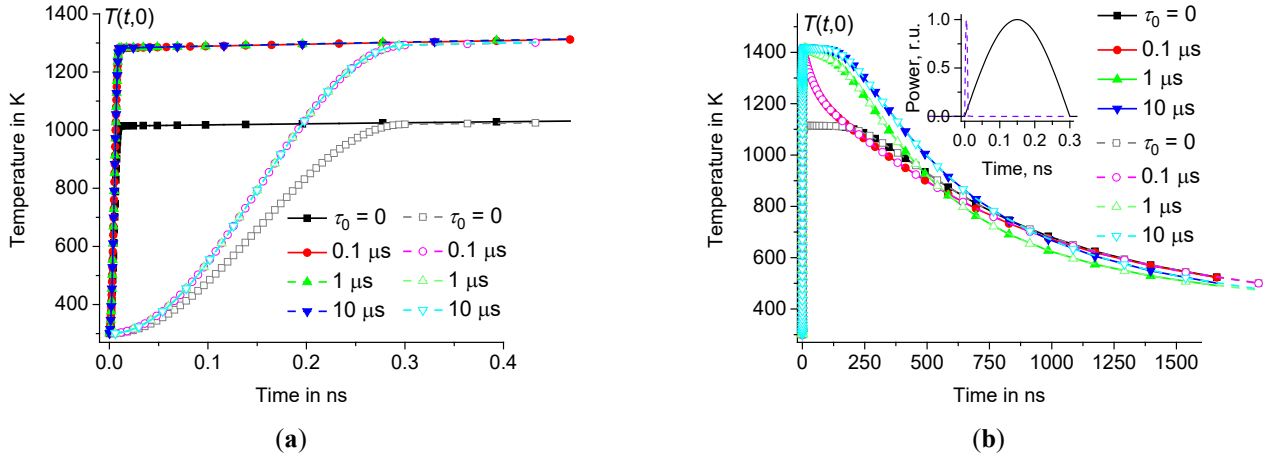


Figure 5. Time dependence of $T(t,0)$ in the center of the hot zone during (a) and after (b) the heating pulse of half-sinusoidal shape at $\tau_p = 10$ ps and 300 ps – filled and open symbols, respectively, at the same parameters as in Figure3 ($\tau_0 = 0, 0.1 \mu$ s, 1μ s, and 10μ s – squares, circles, triangles up, and triangles down, respectively). Inset (b) shows pulse power as a function of time for short and long pulses – dotted and solid lines, respectively.

Thus, the temperature $T(t,0)$ at the center of the hot zone increases very fast over the time interval $(0, \tau_p)$ from T_{in} to the maximum value T_{max} and then relaxes relatively slowly on a microsecond time scale, see Figures4 and 5. The influence of time dispersion of dynamic heat capacity is significant on time scales of several hundred nanoseconds or less. The solution associated with the dynamic heat capacity (at $\tau_0 \neq 0$) tends to the classical solution (corresponding to $\tau_0 = 0$) when t reaches approximately 1μ s, see Figures4(b) – 5(b).

3.2. Comparison with the fundamental solution of the classical problem

It is often believed that the hot focal spot should spread and cool down according to the law $r \sim (D_0 t)^{1/2}$ and $T \sim t^{-3/2}$, respectively [19,47,81,82]. This assumption is based on the fundamental solution of the Fourier heat equation, which can be represented by the following function [83]:

$$G(t, \vec{r}) = \theta(t) \exp(-|\vec{r}|^2 / 4D_0 t) / (4\pi D_0 t)^{3/2}, \quad (11)$$

where $\theta(t)$ is the Heaviside unit step function and r is the distance from the instantaneous point heat source. However, for a non-point heat source, the approximation of $T(t, r)$ by this function is not satisfactory. The real dependence $T(t, r)$ differs significantly from Eq.(11) [46]. As expected, the temperature perturbation $\delta T(t) = T(t, 0) - T_{in}$ in the center of the heating zone relaxes in a time of the order of r_0^2 / D_0 . However, $\delta T(t)$ remains near the maximum value $\delta T(\tau_p)$ at $t < 0.1 \mu$ s (see Figure6), and only then $\delta T(t)$ relaxes over a time of the order of r_0^2 / D_0 . In contrast to the estimate based on the fundamental solution of the Fourier heat equation, the temperature perturbation $\delta T(t)$ relaxes approximately as $T \sim t^{-1}$, and not as $T \sim t^{-3/2}$, see Figure6. In fact, to obtain the correct temperature distribution $T(t, r)$ using the fundamental solution, it is necessary to integrate the thermal response over the time interval $(0, \tau_p)$ and the volume of the heating zone. Thus, for the heat source $\Phi(t, r)$ considered above, distributed in a volume with radius r_0 and acting on the time interval $(0, \tau_p)$, we obtain the temperature distribution $T_{FS}(t, r)$:

$$T_{FS}(t, r) = \int_0^{r_0} \int_0^{\tau_p} \int_0^\pi \frac{\Phi_0 F(\tau)}{\rho c_0} G(t - \tau, \vec{r} - \vec{\xi}) 2\pi \sin(\theta) \xi^2 d\xi d\tau d\theta, \quad (12)$$

where $(\vec{r} - \vec{\xi})^2 = r^2 + \xi^2 - 2r\xi \cos(\theta)$. As expected, the solution $T_{FS}(t, r)$ completely coincides with the temperature distribution $T(t, r)$, calculated using Eqs.(8) – (9) at $\tau_0 = 0$, see Figure6. In contrast,

the simplified estimate $\mathcal{T}(t, r) = N_{cor} \frac{\phi_0}{\rho c_0} G(t, \vec{r}) \tau_p V_0$ is far from the correct $T_{FS}(t, r)$ even for any correction factor N_{cor} , see Figure 6.

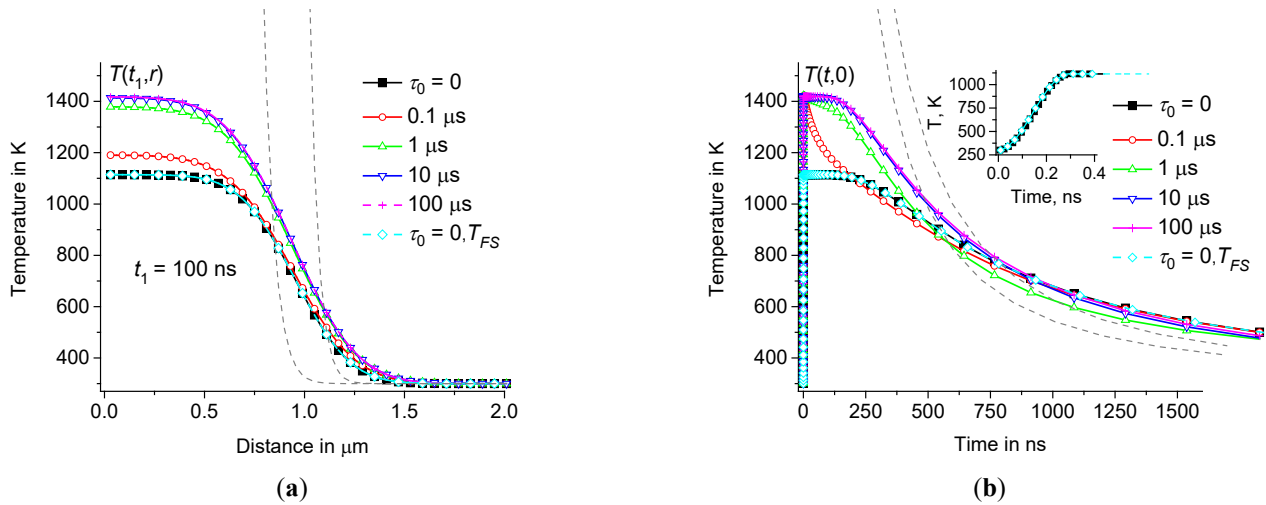


Figure 6. $T(t_1, r)$ depending on the distance r at $t_1 = 100 \text{ ns}$ (a) and time dependence of $T(t, 0)$ in the center of the hot zone (b) at the same parameters as in Figure 3 ($\tau_0 = 0, 0.1 \mu\text{s}, 1 \mu\text{s}, 10 \mu\text{s}$, and $100 \mu\text{s}$ – squares, circles, triangles up, triangles down, and crosses, respectively, as well as $T_{FS}(t, r)$ for $\tau_0 = 0$ – diamonds). Dotted lines show $\mathcal{T}(t_1, r)$ at $N_{cor} = 1$ and 100 (a), as well as $\mathcal{T}(t, 0)$ at $N_{cor} = 1/150$ and $1/200$ (b). Inset (b) shows the initial fragments of $T_{FS}(t, 0)$ and $T(t, 0)$ at $\tau_0 = 0$.

Thus, the correct calculation of the temperature distribution $T(t, r)$ using the fundamental solution of the classical heat equation (without time dispersion) gives the same result as the calculation using Eqs.(8) – (9) at $\tau_0 = 0$. However, using Eqs.(8) – (9) it is possible to calculate the temperature distribution $T(t, r)$ for materials with dynamic heat capacity (at $\tau_0 \neq 0$). It turns out that $T(t, r)$ obtained at $\tau_0 \neq 0$ increases with τ_0 and tends to saturation at τ_0 about $10 \mu\text{s}$, see Figure 6. For this reason, the shape of the distribution function $H(\tau_0)$ has insignificant effect on $T(t, r)$. Next, we consider the influence of this distribution on $T(t, r)$, see Figures 7 – 8.

3.3. Dependence of $T(t, r)$ on the distribution of relaxation times

The influence of the time dispersion of the dynamic heat capacity is most pronounced at the beginning of the heating process on a nanosecond time scale, see Figure 6(b). This effect is significant already at τ_0 about $0.1 \mu\text{s}$, increases with increasing τ_0 and reaches saturation at τ_0 above r_0^2/D_0 , where r_0^2/D_0 is about $4 \mu\text{s}$ at $r_0 = 1 \mu\text{m}$ and $D_0 = 2.6 \cdot 10^{-7} \text{ m}^2/\text{s}$ for borosilicate glass. In fact, in glasses the relaxation times τ_0 are distributed over a wide range. The parameters of the VFTH relationship (see Eq.(5)) can be obtained from measurements of glass transition processes depending on the cooling rate. For example, we use these parameters for borosilicate glass [64], sodium-lime-magnesium-silicate glass [84], and sodium-silicate glass [85]. The relaxation parameters of these silicate glasses used for model calculations are collected in Table 2.

Table 2. Relaxation parameters of silicate glasses used for model calculations.

Substance	f_0 Hz	B K	T_0 K
Boro-silicate glass	$5 \cdot 10^{17}$	$1.9 \cdot 10^4$	392
Sodium-lime-magnesium-silicate glass	$1 \cdot 10^{14}$	$1.1 \cdot 10^4$	480
Sodium-silicate glass	$1.24 \cdot 10^{14}$	$1.29 \cdot 10^4$	407

The dynamic heat capacity $c_{dyn}(t)$ can be modeled using Eq.(4), where $\tau_K(T) = \frac{0.737}{2\pi f_{max}}$ can be obtained from f_{max} (see Eq.(5)) using the relaxation parameters, see Table 2. Thus, we obtain the temperature distribution $T_{AV}(t, r)$ averaged using the distribution function $H(\tau_K(T_{int}))$, where

$\tau_K(T_{int})$ is obtained at several intermediate temperatures between T_{in} and T_{max} (T_{max} is the maximum value of the temperature $T(t, 0)$ at the center of the hot zone). For example, set $T_{int} = 700$ K and 1000 K and consider the relaxation parameters for borosilicate glass [64], sodium-lime-magnesium-silicate glass [84], and sodium-silicate glass [85], see Table 2. The results are presented in Figures 7 – 8. The difference between $T(t, r)$, obtained for sufficiently large $\tau_0 \geq 10 \mu\text{s}$, and $T_{AV}(t, r)$, obtained for $\tau_K(700\text{K})$ and $\tau_K(1000\text{K})$, is insignificant, see Figures 7 – 8. Since the influence of the time dispersion of the dynamic heat capacity reaches saturation at τ_0 about $10 \mu\text{s}$, the shape of the distribution function $H(\tau_0)$ has little effect on the temperature distribution. Thus, the influence of the time dispersion of the dynamic heat capacity on the temperature distribution $T(t, r)$ can be calculated for a fixed, sufficiently large τ_0 .

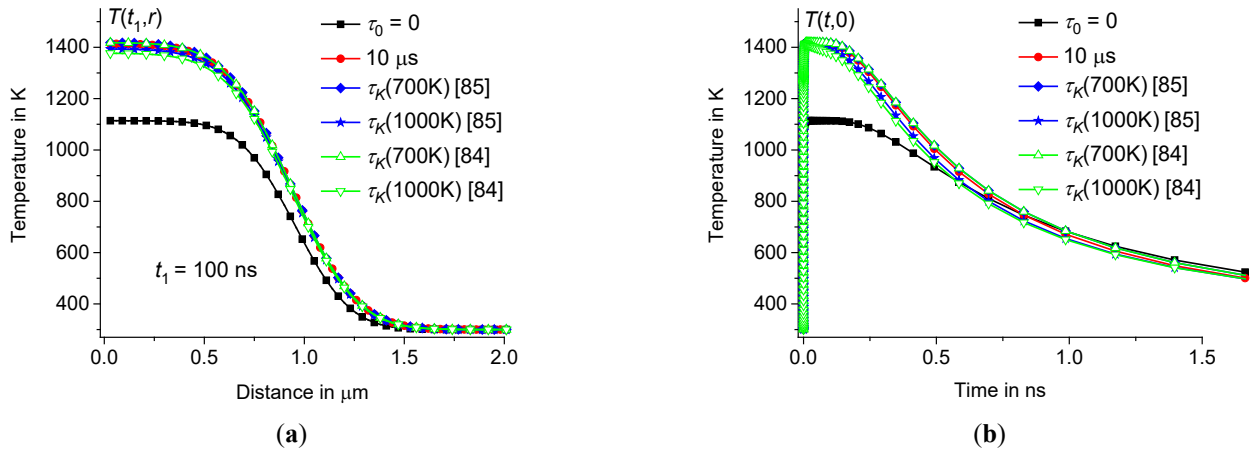


Figure 7. $T(t_1, r)$ depending on the distance r at $t_1 = 100$ ns (a) and time dependence $T(t, 0)$ in the center of the hot zone (b) at the same parameters as in Figure 3 ($\tau_0 = 0$ and $10 \mu\text{s}$ – squares and circles). The temperature distribution $T_{AV}(t, r)$ averaged using the distribution function $H(\tau_K(T_{int}))$ obtained from [85] at $T_{int} = 700$ K and 1000 K – diamonds and stars, as well as from [84] at $T_{int} = 700$ K and 1000 K – triangles up and triangles down, respectively.

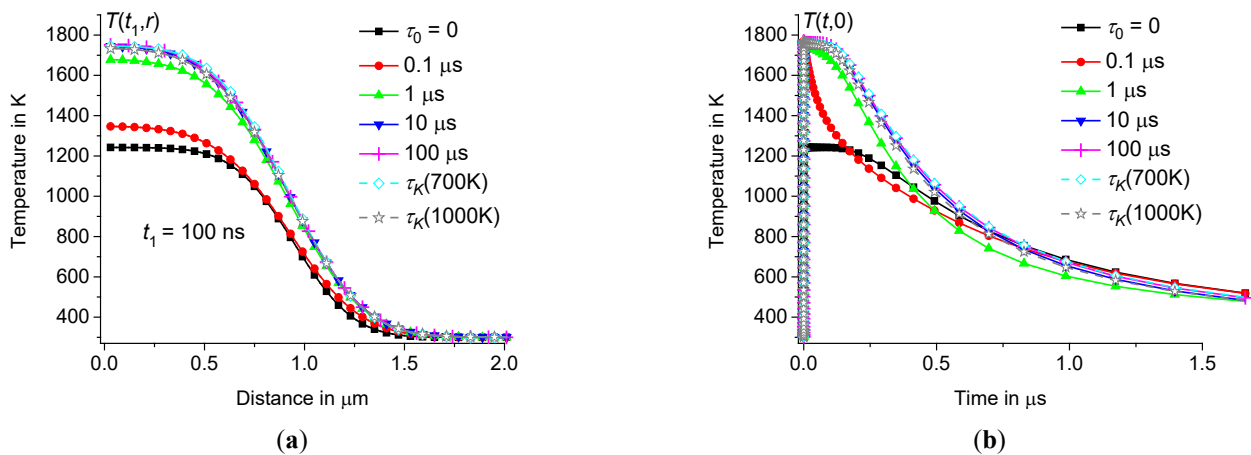


Figure 8. $T(t_1, r)$ depending on the distance r at $t_1 = 100$ ns (a) and time dependence $T(t, 0)$ in the center of the hot zone (b) for borosilicate glass at $r_0 = 1 \mu\text{m}$, $\tau_p = 10$ ps, and $E_p = 15$ nJ ($T_{in} = 300$ K ($\tau_0 = 0, 0.1 \mu\text{s}, 1 \mu\text{s}, 10 \mu\text{s}$, and $100 \mu\text{s}$ – squares, circles, triangles up, triangles down, and crosses). The solution $T_{AV}(t, r)$ averaged using the distribution function $H(\tau_K(T_{int}))$ obtained from [64] at $T_{int} = 700$ K and 1000 K – diamonds and stars.

The influence of time dispersion of dynamic heat capacity is significant in both borosilicate and sodium-silicate glasses. Now let us consider the influence of the size of the heating zone r_0 on the temperature distribution $T(t, r)$.

3.4. Dependence of $T(t, r)$ on the size of the heating zone

For example, let us compare the temperature distributions $T(t, r)$ at $r_0 = 1$ and $r_0 = 2 \mu\text{m}$ for borosilicate glass, see Table 1. To obtain the same thermal response value, let us set $E_p = 120 \text{ nJ}$ at $r_0 = 2 \mu\text{m}$, increasing the energy in proportion to the volume of the heating zone. Thus, in both cases we obtain the same amplitudes of the temperature response to heating pulses, see Figures 8 – 9. As expected, the temperature $T(t, 0)$ in the center of the heating zone relaxes in a time of the order of r_0^2/D_0 , which for borosilicate glass is about $15 \mu\text{s}$ at $r_0 = 2 \mu\text{m}$ and $D_0 = 2.6 \cdot 10^{-7} \text{ m}^2/\text{s}$. For comparison, $T(t, 0)$ relaxes four times faster at $r_0 = 1 \mu\text{m}$ than at $r_0 = 2 \mu\text{m}$, see Figures 8(b) – 9(b). As the size of the heating zone increases, the saturation of the influence of the time dispersion of the dynamic heat capacity on $T(t, r)$ shifts towards larger values of τ_0 . For example, compare $T(t, r)$ at $\tau_0 = 1 \mu\text{s}$ for $r_0 = 1$ and $r_0 = 2 \mu\text{m}$, see Figures 8 – 9.

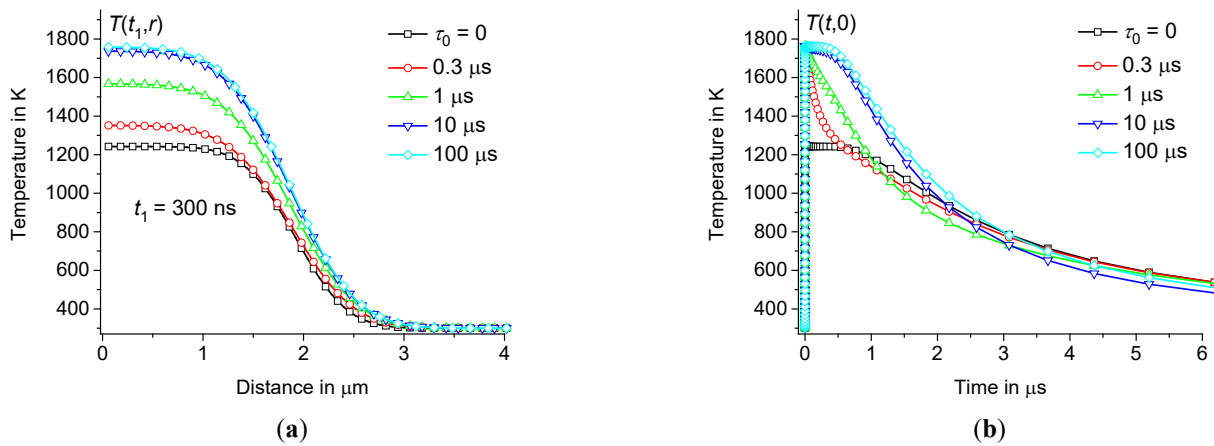


Figure 9. $T(t_1, r)$ depending on the distance r at $t_1 = 300 \text{ ns}$ (a) and time dependence of $T(t, 0)$ in the center of the hot zone (b) for borosilicate glass at $r_0 = 2 \mu\text{m}$, $\tau_p = 300 \text{ ps}$, $E_p = 120 \text{ nJ}$, $T_{in} = 300 \text{ K}$ ($\tau_0 = 0, 0.3 \mu\text{s}, 1 \mu\text{s}, 10 \mu\text{s},$ and $100 \mu\text{s}$ – squares, circles, triangles up, triangles down, and diamonds).

4. Cooling rate distribution $-\mathcal{R}(t, r)$ and its influence on microstructuring processes of glasses

Now consider the spatial distribution of the rate of temperature change $\mathcal{R}(t, r)$. Due to thermal expansion, the size of the heating zone changes with temperature by about 10 nm or less. We neglect these changes with respect to r_0 . Let us consider the rate of temperature change $\mathcal{R}(t, r) = \frac{\partial T(t, r)}{\partial t}$ due to thermal diffusion. This temperature change affects the physical properties of the material. We will focus on very fast (about 10^9 K/s or more) local temperature changes that have the greatest impact on the microstructuring process, and will study the effect associated with the time dispersion of the dynamic heat capacity. It is worth noting that this effect is significant even well above the glass transition temperature T_g .

For example, the rate of temperature change $\mathcal{R}(t, r)$ for borosilicate glass at $r_0 = 2 \mu\text{m}$, $\tau_p = 300 \text{ ps}$, $E_p = 120 \text{ nJ}$ and various τ_0 is presented in Figures 10 – 11. Note that the rate of temperature change $\mathcal{R}(t, r)$ is greatest near the periphery of the hot zone, see Figure 10(a). The cooling rate $-\mathcal{R}(t, r)$ is about 600 GK/s at $r_1 = 1.98 \mu\text{m}$ and $t_1 = 0.36 \text{ ns}$, see Figure 11(a). However, in the center of the heating zone, the cooling rate $-\mathcal{R}(t, 0)$ does not exceed 0.6 GK/s, i.e. $-\mathcal{R}(t, 0)$ is three orders of magnitude less than the cooling rate at the periphery, see Figure 11. Therefore, the local structure of glass in the center of the hot zone should differ significantly from the structure at the periphery of the heating zone after laser modification. This conclusion is consistent with experiments [19,34,36,40,46,49–53]. However, the effect associated with dynamic heat capacity (at $\tau_0 \neq 0$) is significant both in the center and at the periphery of the heating zone. Indeed, the maximum cooling rate is approximately 2.5 times greater at $\tau_0 \neq 0$ than at $\tau_0 = 0$ both at the periphery and in the center of the heating zone, see Figure 11.

Let us consider the cooling rate $-\mathcal{R}(t, r)$ in a thin shell in the region from $0.95r_0$ to $0.99r_0$. As we have established for borosilicate and sodium-lime-silicate glasses, ultra-fast cooling of the material occurs in this region at a rate of more than 10^{11} K/s, see Figures 10 – 13. It is noteworthy that at the beginning of the cooling process (during the first few nanoseconds), the rate of temperature change $\mathcal{R}(t, r)$ is the same for small and large relaxation times τ_0 , see Figures 10(a) and 12(a). This means that at the beginning of the cooling process at the periphery of the hot zone, the shape of the distribution function $H(\tau_0)$ does not affect the cooling rate $-\mathcal{R}(t, r)$. Therefore, in this case, even at very small relaxation times τ_0 , the influence of the time dispersion of the dynamic heat capacity is significant.

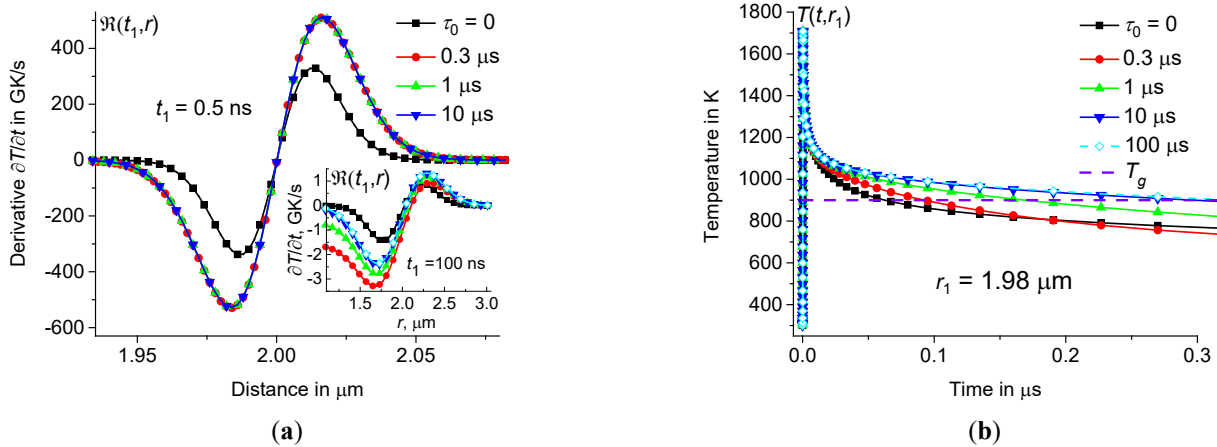


Figure 10. Rate of temperature change $\mathcal{R}(t_1, r)$ depending on the distance r at the periphery of the hot zone at $t_1 = 0.5$ ns (a) and time dependence of $T(t, r_1)$ at $r_1 = 1.98$ μm (b) at the same parameters as in Figure 9 ($\tau_0 = 0, 0.3$ $\mu\text{s}, 1$ $\mu\text{s}, 10$ μs , and 100 μs – squares, circles, triangles up, triangles down, and diamonds). Inset (a) shows $\mathcal{R}(t_1, r)$ as a function of distance r at $t_1 = 100$ ns for different τ_0 .

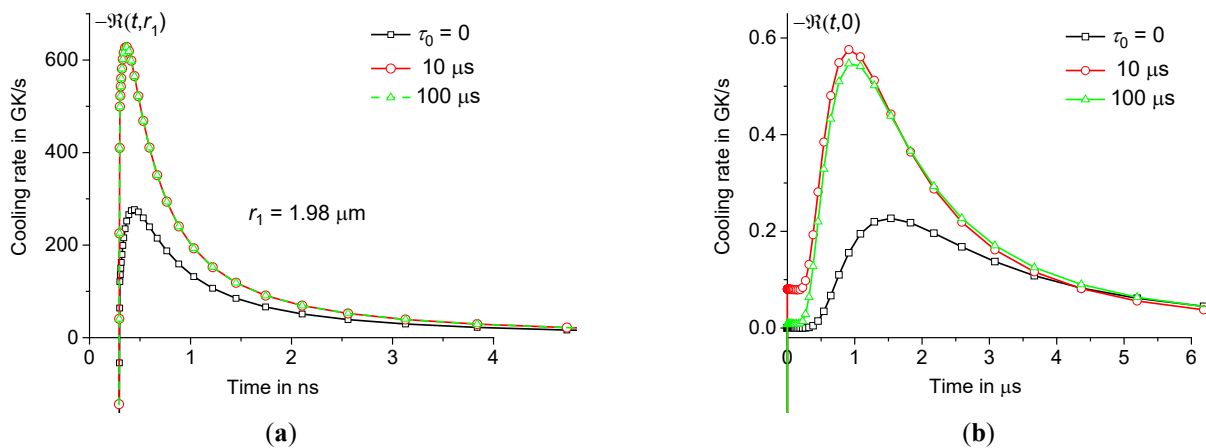


Figure 11. Time dependence of cooling rate $-\mathcal{R}(t, r_1)$ at $r_1 = 1.98$ μm (a) and $r_1 = 0$ (b) at the same parameters as in Figures 9 and 10 ($\tau_0 = 0, 10$ μs , and 100 μs – squares, circles, and triangles).

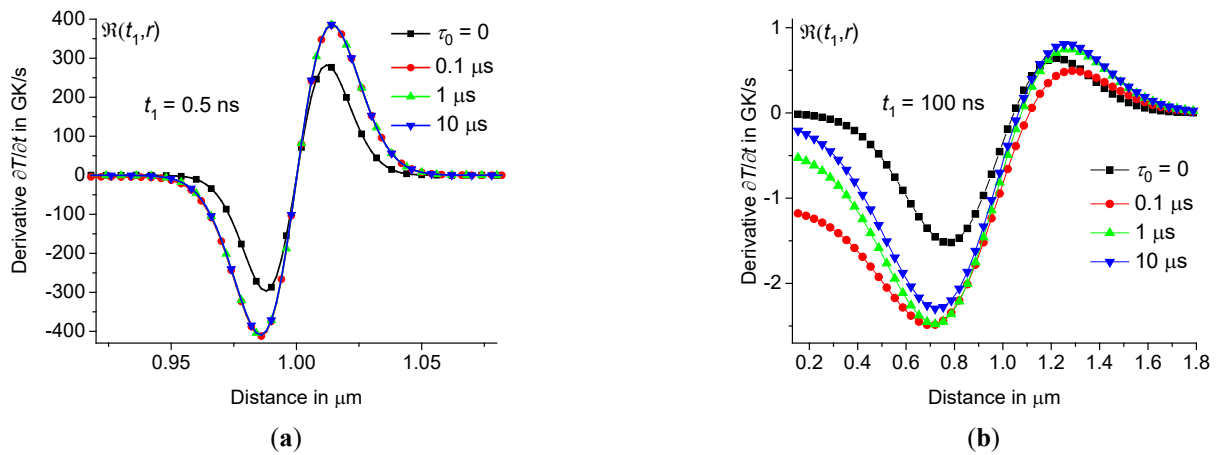


Figure 12. $\mathcal{R}(t_1, r)$ depending on the distance r at the periphery of the hot zone at $t_1 = 0.5$ ns (a) and $t_1 = 100$ ns (b) for sodium-lime-silicate glass at the same parameters as in Figure3 ($\tau_0 = 0, 0.1 \mu\text{s}, 1 \mu\text{s},$ and $10 \mu\text{s}$ – squares, circles, triangles up, and triangles down).

The cooling rate $-\mathcal{R}(t_1, r)$ reaches a maximum at r_{max} for a given t_1 , see Figures10 and 12. The rate $-\mathcal{R}(t, r_{max})$ decreases over time, and the distance r_{max} , at which the rate $-\mathcal{R}(t, r_{max})$ is maximum, shifts slightly towards the center of the heating zone. However, $-\mathcal{R}(t, r_{max})$ still exceeds 2–3 GK/s at $t_1 = 100$ ns, see Figures10(a) and 12(b). The change in cooling rate $-\mathcal{R}(t, r_{max})$ over time for sodium-lime-silicate glass at $r_0 = 1 \mu\text{m}$, $\tau_0 = 10 \mu\text{s}$ and the same conditions as in Figure3 is presented in Table 3. The rate $\mathcal{R}(t_1, r)$ depending on the distance r at the periphery of the hot zone for different t_1 is shown in Figure13.

Table 3. Cooling rate $-\mathcal{R}(t, r)$ for sodium-lime-silicate glass at $r_0 = 1 \mu\text{m}$.

Time t_1 ns	Distance r_{max} μm	Cooling rate $-\mathcal{R}(t_1, r_{max})$ GK/s
0.5	0.985	410
1	0.98	170
5	0.94	31
10	0.92	16
50	0.80	4
100	0.70	2.3

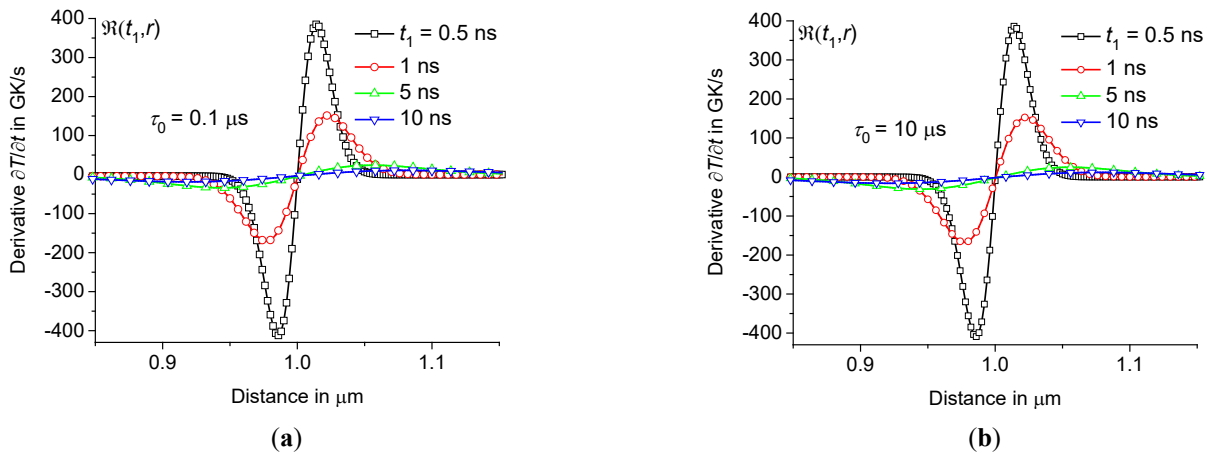


Figure 13. $\mathcal{R}(t_1, r)$ depending on the distance r at the periphery of the hot zone at $\tau_0 = 0.1 \mu\text{s}$ (a) and $\tau_0 = 10 \mu\text{s}$ (b) at the same parameters as in Figure3 ($t_1 = 0.5 \text{ ns}$, 1 ns , 5 ns , and 10 ns – squares, circles, triangles up, and triangles down).

Thus, since the local structure of the material strongly depends on the local cooling rate $-\mathcal{R}(t, r)$, the local structure of the material at the periphery of the hot zone changes significantly relative to the original glass matrix. This modification of glass practically stops as soon as the local region is cooled below the glass transition temperature T_g . Thus, the modification process occurs until the temperature $T(t, r_1)$ in the local region at $r = r_1$ drops below T_g . For example, consider the cooling curves calculated at the periphery of the hot zone for borosilicate ($T_g = 900 \text{ K}$ [63]) and sodium-lime-silicate glasses ($T_g = 840 \text{ K}$ [57]), see Figure10(b) and Figure14, respectively. It should be noted that the effect associated with the time dispersion of the dynamic heat capacity is significant well above the glass transition temperature T_g . Indeed, in the case of $r_0 = 1 \mu\text{m}$, the modification process occurs within approximately 80 ns at $r_1 = 0.95 \mu\text{m}$ and $\tau_0 \geq 1 \mu\text{s}$, see Figure14(a). However, without taking into account the time dispersion of the dynamic heat capacity (at $\tau_0 = 0$), this process occurs in less than 20 ns , see Figure14(a). In the case of $r_0 = 2 \mu\text{m}$, the modification process occurs during a longer period of about 300 ns at $r_1 = 1.98 \mu\text{m}$ and $\tau_0 > 1 \mu\text{s}$, see Figure10(b). However, without taking into account the time dispersion of the dynamic heat capacity (at $\tau_0 = 0$), this process occurs in less than 50 ns , see Figure10(b).

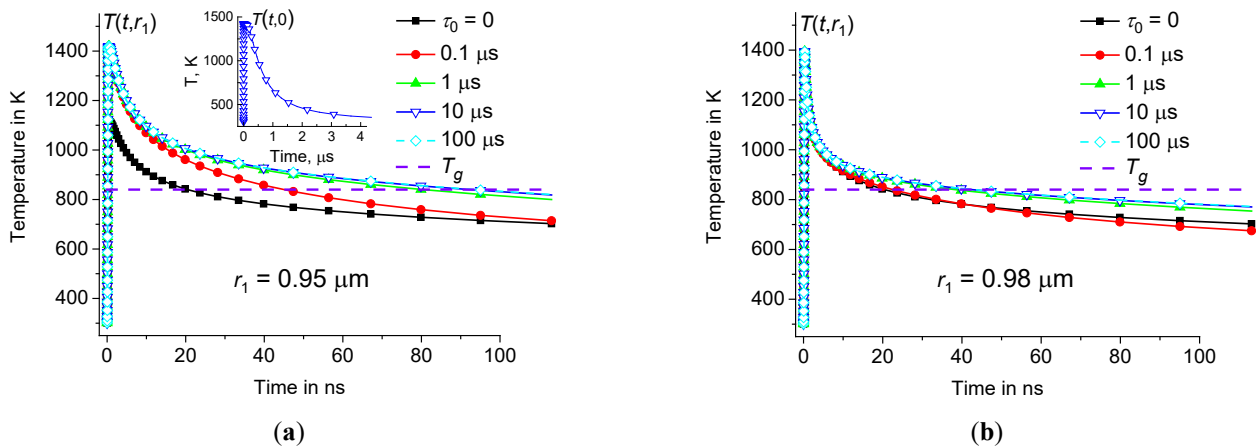


Figure 14. Time dependence of $T(t, r_1)$ at the periphery of the hot zone at $r_1 = 0.95 \mu\text{m}$ (a) and $r_1 = 0.98 \mu\text{m}$ (b) at the same parameters as in Figure3 ($\tau_0 = 0, 0.1 \mu\text{s}, 1 \mu\text{s}, 10 \mu\text{s}$, and $100 \mu\text{s}$ – squares, circles, triangles up, triangles down, and diamonds). Inset (a) shows time dependence of $T(t, 0)$ in the center of heating zone (at $\tau_0 = 10 \mu\text{s}$).

To summarize, we can conclude that the maximum cooling rate exists in the outer regions of the heating zone, in the shell of about $(0.97 \pm 0.02)r_0$. The cooling rate reaches several hundred GK/s in the first nanosecond after the laser pulse. Then the cooling rate decreases. However, even 100 ns after the laser pulse, $-\mathcal{R}(t, r)$ in the outer shell of the hot zone still exceeds 1 GK/s . It is noteworthy that in the center of the heating zone the cooling rate is three orders of magnitude less than $-\mathcal{R}(t, r)$ at the periphery. Since regions quenched at different cooling rates have different physical properties, strong gradients of physical properties should exist in the material predominantly at a distance of about $0.9r_0$ from the center of the heating zone. This effect is significantly enhanced by the time dispersion of the dynamic heat capacity.

In conclusion, let us briefly discuss laser micro-processing in the cumulative heating mode. Typically, cumulative heating is achieved at a laser pulse repetition rate more than hundreds of kHz. Usually, this mode operates at frequencies from 200 kHz to 10 MHz [3]. Indeed, the temperature $T(t, 0)$ in the center of the hot zone relaxes in a time of the order of r_0^2/D_0 , which for the glasses under consideration is about $4 \mu\text{s}$ at $r_0 = 1 \mu\text{m}$, see inset in Figure14(a). Thus, in this case, the cumulative effect can be achieved at a frequency of about 250 kHz or more. Note that the cumulative effect leads

to stable average heating of the material in the heating zone. Thus, the effect of laser pulse repetition can be approximately simulated by shifting upward the local temperature distribution $T(t, r)$ by a certain temperature difference ΔT , which increases with increasing pulse repetition frequency. It is clear that with increasing ΔT the modification process will occur over a longer time interval, see Figure 14, where $T(t, r_1)$ should be shifted upward by the amount ΔT . Then $T(t, r_1)$ in the local region at $r = r_1$ will fall below T_g at a cooling rate lower than at zero repetition frequency (at $\Delta T = 0$). Consequently, local gradients in the physical properties of locally modified glass will be smoothed out due to cumulative heating. The effect of the repetition rate will be discussed in more detail in a separate article.

5. Discussion

The local temperature distribution $T(t, r)$ and the local cooling rate $-\mathcal{R}(t, r)$ determine the local structure of the glass matrix during laser-induced microstructuring. Thus, knowledge of the dynamics of the local temperature distribution $T(t, r)$ is very important for applications associated with local laser heating, for example, for femtosecond laser microstructuring of glasses. However, as shown in this article, the dynamics of the local temperature distribution $T(t, r)$ significantly depends on the time dispersion of the dynamic heat capacity $c_{dyn}(t)$ of the glass matrix. This work proposes a method for analytical calculation of $T(t, r)$ and $\mathcal{R}(t, r)$ for glass-forming materials under local fast laser excitations. It is shown that the dynamics of the local temperature distribution $T(t, r)$ caused by a laser pulse can be described by the heat equation with dynamic heat capacity $c_{dyn}(t)$. This equation has an analytical solution to a spherically symmetric boundary value problem. Using this analytical solution, we obtained the temperature distribution $T(t, r)$ and local cooling rate $-\mathcal{R}(t, r)$ for the thermal parameters of borosilicate and sodium-lime-silicate glasses. In fact, this analytical solution depends on the following relaxation parameters of the dynamic heat capacity $c_{dyn}(t)$ of the material: relaxation time τ_0 and the distribution function $H(\tau_0)$, which can be obtained from broadband heat capacity spectroscopy. However, as shown in this article, the shape of the distribution function $H(\tau_0)$ has little effect on $T(t, r)$ and $\mathcal{R}(t, r)$, since with increasing τ_0 the influence of the time dispersion of the dynamic heat capacity $c_{dyn}(t)$ reaches saturation. It should be noted that the influence of the time dispersion of the dynamic heat capacity is most pronounced at the beginning of the process, when t changes on a nanosecond time scale. We found that this effect is significant already at τ_0 about 0.1 μs , increases with increasing τ_0 and reaches saturation at τ_0 above r_0^2/D_0 . Thus, the influence of the time dispersion of dynamic heat capacity on the temperature distribution $T(t, r)$ can be calculated for a fixed, sufficiently large τ_0 (in fact, for τ_0 of the order of ten or several tens of microseconds, depending on the radius of the heating zone r_0). As expected, the results obtained are very similar for different r_0 . However, as the size of the heating zone increases, the laser pulse energy E_p must increase in proportion to the volume V_0 of the heating zone in order to obtain the same amplitude of the local thermal response.

It has been established that the temperature distribution $T(t, r)$ and local cooling rate $-\mathcal{R}(t, r)$ are not affected by the heating pulse duration τ_p and the shape of the heating pulse. It should be noted that the temperature perturbation $\delta T(t) = T(t, 0) - T_{in}$ in the center of the heating zone relaxes not as $\delta T \sim t^{-3/2}$, in contrast to the often-used estimate based on the fundamental solution of the Fourier heat equation. In fact, the heating pulse cannot be considered as an instantaneous point source of heat. Thus, it is necessary to integrate the thermal response over the time interval $(0, \tau_p)$ and the volume of the heating zone, then the resulting correct solution $T_{FS}(t, r)$ completely coincides with the temperature distribution $T(t, r)$ found in this article for $\tau_0 = 0$. In addition, the solution found in this article can be used for materials with dynamic heat capacity $c_{dyn}(t)$ at $\tau_0 \neq 0$.

We found that the rate of temperature change $\mathcal{R}(t, r)$ is greatest near the periphery of the hot zone. The cooling rate reaches a maximum $-\mathcal{R}(t, r_{max})$ when r_{max} is slightly less than r_0 . It turns out that ultra-fast cooling of the material occurs at a rate of more than 10^{11} K/s in a thin shell in the region from $0.95r_0$ to $0.99r_0$. However, in the center of the heating zone, the cooling rate is three orders of magnitude lower than at the periphery. Thus, the local structure of glass after laser modification in the center of the hot zone should differ significantly from the structure at the

periphery, which is consistent with experiments [19,34,36,40,46,49–53]. It is noteworthy that the effect associated with the time dispersion of the dynamic heat capacity is very significant both in the center and at the periphery of the heating zone. In fact, the maximum cooling rate is approximately 2.5 times greater at $\tau_0 \neq 0$ than at $\tau_0 = 0$ both at the periphery and in the center of the heating zone, see Figure 11.

It is worth noting that at the beginning of the cooling process at the periphery of the hot zone, the shape of the distribution function $H(\tau_0)$ does not affect the cooling rate $-\mathcal{R}(t, r)$. In fact, even at a very short relaxation time τ_0 , the influence of the time dispersion of the dynamic heat capacity is very significant at the beginning of the cooling process. The cooling rate decreases over time t , however, in the outer regions of the heating zone, the cooling rate $-\mathcal{R}(t, r)$ still exceeds 2–3 GK/s at t about 100 ns. Regions quenched at different cooling rates have different physical properties. Thus, strong gradients of physical properties should exist in the material, mainly at a distance of about $0.9r_0$ from the center of the heating zone. It is worth noting that the time dispersion of the dynamic heat capacity significantly enhances this effect. In addition, the effect associated with the time dispersion of the dynamic heat capacity is significant even well above the glass transition temperature T_g . It turns out that the duration of the modification process strongly depends on the relaxation time τ_0 of the dynamic heat capacity $c_{dyn}(t)$. Thus, the rate of local cooling and gradients of physical properties of locally modified glass strongly depend on the relaxation time of the dynamic heat capacity $c_{dyn}(t)$. Finally, it is worth noting that the gradients of physical properties in areas quenched at different cooling rates are smoothed out by cumulative heating when processed in the cumulative heating mode.

In this article, we solved a problem for spherical geometry, which is closely related to data storage technologies. There are a number of future directions that are worth developing. A future research direction could be the problem with cylindrical geometry, closely related to laser waveguide technologies. The cumulative heating mode at different laser pulse repetition rates and laser beam scanning speeds also deserves to be studied.

6. Conclusions

To summarize, it can be emphasized that during laser microstructuring of glass-forming materials, the local temperature distribution $T(t, r)$ and the local cooling rate significantly depend on the time dispersion of the dynamic heat capacity $c_{dyn}(t)$ of the glass matrix. The rate of temperature change $\mathcal{R}(t, r)$ is maximum near the periphery of the heating zone. However, the effect associated with the time dispersion of the dynamic heat capacity is very significant both in the center and at the periphery of the heating zone. The effect associated with the time dispersion of the dynamic heat capacity is significant even well above the glass transition temperature T_g . It turns out that in the thin shell of the heating zone, ultra-fast cooling of the material occurs at a rate of more than 10^{11} K/s, and strong gradients of physical properties must exist in the material, mainly in a thin shell around the heating zone. The time dispersion of the dynamic heat capacity significantly enhances this effect. However, these gradients in physical properties should be smoothed out when processed in the cumulative heating mode. Further directions of research may be related to the consideration of the cumulative heating regime for various geometries. The results of this work can be useful for a better understanding and optimization of technologies associated with laser-induced microstructuring of glasses.

Author Contributions: Conceptualization, A.M.; formal analysis, A.M.; methodology, A.M.; supervision, C.S.; visualization, A.M.; writing—original draft, A.M.; writing—review and editing, C.S. All authors have read and agreed to the published version of the manuscript.

Funding: This research received no external funding.

Institutional Review Board Statement: Not applicable.

Informed Consent Statement: Not applicable.

Data Availability Statement: The datasets generated during and/or analyzed during the current study are available from the corresponding author on reasonable request.

Acknowledgments: A.M. acknowledges the administrative and technical support of the Prokhorov General Physics Institute of the Russian Academy of Sciences.

Conflicts of Interest: The authors declare no conflicts of interest.

Nomenclature

Latin Symbols

B and T_0	Parameters of the VFTH equation (K)
c_S	Heat capacity of the solid material ($J \cdot kg^{-1} \cdot K^{-1}$)
c_L	Heat capacity of the liquid material ($J \cdot kg^{-1} \cdot K^{-1}$)
c_{in}, c_0	Initial and equilibrium heat capacities ($J \cdot kg^{-1} \cdot K^{-1}$)
$c_{dyn}(t)$	Dynamic heat capacity ($J \cdot kg^{-1} \cdot K^{-1}$)
D_0	Thermal diffusivity $\lambda/\rho c_0$ ($m^2 \cdot s^{-1}$)
E_p	Energy of laser pulse (nJ)
f_0	Parameter of the VFTH equation (Hz)
$F(t)$	Time dependence of the pulse power (dimensionless)
$G(t, \vec{r})$	Fundamental solution of the Fourier heat equation (m^{-3})
$H(\tau_0)$	Distribution function (s^{-1})
K_B	Bulk modulus (GPa)
$\mathcal{R}(t, r)$	Rate of temperature change $\mathcal{R}(t, r) = \partial T(t, r)/\partial t$ ($K \cdot s^{-1}$)
$-\mathcal{R}(t, r)$	Cooling rate ($K \cdot s^{-1}$)
R_0	Parameter of the boundary value problem (μm)
r_0	Heating zone radius (μm)
r	Distance from the center of the hot zone (μm)
t	Time (s)
$T_{FS}(t, r)$	Temperature distribution obtained from fundamental solution (K)
$T(t, r)$	Local temperature distribution (K)
$T_{AV}(t, r)$	Temperature distribution averaged using $H(\tau_0)$ (K)
T_g	Glass transition temperature (K)
T_{in}	Initial temperature (K)
T_{int}	Intermediate temperature (K)
T_{max}	Maximum value of $T(t, r)$ (K)
V_0	Heating zone volume (m^3)
V	Specific volume ($m^3 \cdot kg^{-1}$)
V_L	Longitudinal speed of sound ($m \cdot s^{-1}$)

Greek Symbols

α	Linear thermal expansion (K^{-1})
α_V	Volumetric thermal expansion coefficient (K^{-1})
β	Parameter of the Kohlrausch relaxation law (dimensionless)
γ_n	Relaxation parameter (dimensionless)
ε_0	Coefficient $\varepsilon_0 = (c_0 - c_{in})/c_0$ (dimensionless)
λ	Thermal conductivity ($W \cdot m^{-1} \cdot K^{-1}$)
μ_n	Relaxation parameter (dimensionless)
ρ	Density ($kg \cdot m^{-3}$)
τ_0	Debye relaxation time (μs)
τ_K	Kohlrausch relaxation time (μs)
τ_{laser}	Duration of laser pulse (fs)
τ_n	nth relaxation time (μs)
τ_p	Duration of heating pulse (ps)
$\Phi(t, r)$	Volumetric heat flux density ($W \cdot m^{-3}$)
Φ_0	Volumetric heat flux density ($W \cdot m^{-3}$)
Φ_n	nth Fourier component ($W \cdot m^{-2}$)
$\psi_n(t)$	nth Fourier component ($K \cdot m$)
ω	Temperature modulation frequency ($rad \cdot s^{-1}$)

Appendix A

Eq.(7) can be converted to Eq.(13) by replacing $r(T(t, r) - T_{in})$ with $U(t, r)$:

$$U'(t, r) - D_0 \partial^2 U / \partial r^2 = \frac{r \Phi(r) F(t)}{\rho c_0} + \varepsilon_0 \frac{\partial}{\partial t} \int_0^t \exp\left(-\frac{t-\tau}{\tau_0}\right) U'(\tau, r) d\tau, \quad (13)$$

Thus, we obtain a one-dimensional problem, with uniform boundary and initial conditions: $U(t, 0) = 0$, $U(t, R_0) = 0$, and $U(t, r) = 0$ at $t \leq 0$.

This boundary value problem is satisfied by the following series:

$$U(t, r) = \sum_{n=1} \psi_n(t) \sin(\pi n r / R_0), \quad (14)$$

where the functions $\psi_n(t)$ are the solutions of Eq.(9) [70]. Thus, for a heat source uniformly distributed in a volume of radius r_0 with power density Φ_0 , and for the heating pulse $\Phi_0 \sin(\pi t / \tau_p)$, acting during the time interval τ_p , we obtain solutions $\psi_n(t)$ of Eq.(9) represented by Eq.(15) and Eq.(16) for $0 \leq t \leq \tau_p$ and $\tau_p < t$, respectively.

$$\psi_n(t) = \frac{\Phi_n \tau_n \gamma_n \mu_n}{\rho c_0 (\gamma_n - \mu_n)} \left[\frac{(\gamma_n \tau_0 - 1) \left[\gamma_n \sin(\pi t / \tau_p) + \frac{\pi}{\tau_p} (\exp(-\gamma_n t) - \cos(\pi t / \tau_p)) \right]}{(\gamma_n)^2 + \left(\frac{\pi}{\tau_p}\right)^2} + \frac{(1 - \mu_n \tau_0) \left[\mu_n \sin(\pi t / \tau_p) + \frac{\pi}{\tau_p} (\exp(-\mu_n t) - \cos(\pi t / \tau_p)) \right]}{(\mu_n)^2 + \left(\frac{\pi}{\tau_p}\right)^2} \right], \quad (15)$$

$$\psi_n(t) = \frac{\Phi_n \pi \tau_n \gamma_n \mu_n}{\rho c_0 \tau_p (\gamma_n - \mu_n)} \left[\frac{(\gamma_n \tau_0 - 1) [\exp(-\gamma_n t) + \exp(\gamma_n (\tau_p - t))]}{(\gamma_n)^2 + \left(\frac{\pi}{\tau_p}\right)^2} + \frac{(1 - \mu_n \tau_0) [\exp(-\mu_n t) + \exp(\mu_n (\tau_p - t))]}{(\mu_n)^2 + \left(\frac{\pi}{\tau_p}\right)^2} \right], \quad (16)$$

where $-\gamma_n$ and $-\mu_n$ are the roots of the polynomial $(1 - \varepsilon_0)p^2 + p(\tau_n^{-1} + \tau_0^{-1}) + \tau_n^{-1}\tau_0^{-1}$. The parameters γ_n and μ_n are real, positive, and $(\gamma_n - \mu_n) \neq 0$ for $0 < \varepsilon_0 < 1$ and $0 < \tau_n, \tau_0$. The series in Eq.(8) converges as $1/n^2$ for $\tau_p < t$. In fact, it is enough to calculate the sum in Eq.(8) to about a thousand terms to obtain a result with an error of less than 1%.

Similarly, for a heating pulse of a square shape with power density Φ_0 , acting on a time interval τ_p , we obtain $\psi_n(t) = \phi_n(t)$ and $\psi_n(t) = [\phi_n(t) - \phi_n(\tau_p - t)]$ for $\tau_p < t$ and $0 \leq t \leq \tau_p$, respectively, where $\phi_n(t)$ are represented by Eq.(17):

$$\phi_n(t) = \frac{\Phi_n \tau_n}{\rho c_0} \left[1 + \frac{\tau_0 \gamma_n \mu_n (\exp(-\mu_n t) - \exp(-\gamma_n t))}{(\gamma_n - \mu_n)} + \frac{\mu_n \exp(-\gamma_n t) - \gamma_n \exp(-\mu_n t)}{(\gamma_n - \mu_n)} \right]. \quad (17)$$

Note that the solutions $\phi_n(t)$ continuously transform into solutions of the classical Fourier heat equation: $\phi_n(t) \rightarrow \frac{\Phi_n}{\rho c_0} \tau_n [1 - \exp(-t/\tau_n)]$ as $\varepsilon_0 \rightarrow 0$ or/and $\tau_0 \rightarrow 0$.

Similarly, the functions $\psi_n(t)$ represented by Eq.(15) and Eq.(16) continuously transform into solutions of the classical Fourier heat equation as $\varepsilon_0 \rightarrow 0$ or/and $\tau_0 \rightarrow 0$, see Eq.(18) and Eq.(19) for $0 \leq t \leq \tau_p$ and $\tau_p < t$, respectively.

$$\psi_n(t) = \frac{\Phi_n \frac{1}{\tau_n} \sin(\pi t / \tau_p) + \frac{\pi}{\tau_p} [\exp(-t/\tau_n) - \cos(\pi t / \tau_p)]}{\rho c_0 \left[\left(\frac{1}{\tau_n}\right)^2 + \left(\frac{\pi}{\tau_p}\right)^2 \right]}, \quad (18)$$

$$\psi_n(t) = \frac{\Phi_n \pi}{\rho c_0 \tau_p} \frac{[\exp(-t/\tau_n) + \exp((\tau_p - t)/\tau_n)]}{\left(\frac{1}{\tau_n}\right)^2 + \left(\frac{\pi}{\tau_p}\right)^2}. \quad (19)$$

References

- Zhang, B.; Wang, Z.; Tan, D.; Liu, X.; Xu, B.; Tong, L.; Kazansky, P.G.; Qiu, J. Ultrafast Laser Inducing Continuous Periodic Crystallization in the Glass Activated via Laser-Prepared Crystallite-Seeds. *Adv. Optical Mater.* 2021, 9, 2001962. <https://doi.org/10.1002/adom.202001962>
- Osellame, R.; Hoekstra, H.J.W.M.; Cerullo, G.; Pollnau, M. Femtosecond laser microstructuring: an enabling tool for optofluidic lab-on-chips. *Laser Photonics Rev.* 2011, 5, 442–463. <https://doi.org/10.1002/lpor.201000031>
- Lei, Y.; Wang, H.; Shayeganrad, G.; Kazansky, P.G. Ultrafast laser nanostructuring in transparent materials for beam shaping and data storage. *Optical Materials Express* 2022, 12, 3327–3355. <https://doi.org/10.1364/OME.463151>
- Stoian, R.; Colombier, J.P. Advances in ultrafast laser structuring of materials at the nanoscale. *Nanophotonics* 2020, 9, 4665–4688. <https://doi.org/10.1515/nanoph-2020-0310>

5. Butkute, A.; Jonusauskas, L. 3D Manufacturing of Glass Microstructures Using Femtosecond Laser. *Micromachines* 2021, 12, 499. <https://doi.org/10.3390/mi12050499>
6. Petit, Y.; Danto, S.; Guerineau, T.; Khalil, A.A.; Camus, A.; Fargin, E.; Duchateau, G.; Berube, J.P.; Vallee, R.; Messaddeq, Y.; Cardinal, T.; Canioni, L. On the femtosecond laser-induced photochemistry in silver-containing oxide glasses: mechanisms, related optical and physico-chemical properties, and technological applications. *Adv. Opt. Techn.* 2018, 7, 291–309. <https://doi.org/10.1515/aot-2018-0037>
7. Torun, G.; Yadav, A.; Richardson, K.A.; Bellouard, Y. Ultrafast Laser Direct-Writing of Self-Organized Microstructures in Ge-Sb-S Chalcogenide Glass. *Front. Phys.* 2022, 10, 883319. <https://doi.org/10.3389/fphy.2022.883319>
8. Lipatiev, A.S.; Lotarev, S.V.; Lipateva, T.O.; Fedotov, S.S.; Lopatina, E.V.; Sigaev, V.N. Ultrafast-Laser-Induced Tailoring of Crystal-in-Glass Waveguides by Precision Partial Remelting. *Micromachines* 2023, 14, 801. <https://doi.org/10.3390/mi14040801>
9. Lipatiev, A.; Lotarev, S.; Lipateva, T.; Okhrimchuk, A.; Fedotov, S.; Lotnyk, A.; Sigaev, V. Fabrication of single-mode hybrid crystal-glass waveguides by direct femtosecond laser writing and thermal annealing. *Materials Research Bulletin* 2022, 152, 111840. <https://doi.org/10.1016/j.materresbull.2022.111840>
10. Beresna, M.; Gecevicius, M.; Kazansky, P.G. Ultrafast laser direct writing and nanostructuring in transparent materials. *Advances in Optics and Photonics* 2014, 6, 293-339. <https://doi.org/10.1364/AOP.6.000293>
11. Shakhgildyan, G.Yu.; Lipatiev, A.S.; Fedotov, S.S.; Vetchinnikov, M.P.; Lotarev, S.V.; Sigaev, V.N. Microstructure and optical properties of tracks with precipitated silver nanoparticles and clusters inscribed by the laser irradiation in phosphate glass. *Ceramics International* 2021, 47, 14320–14329. <https://doi.org/10.1016/j.ceramint.2021.02.012>
12. Jurgens P.; Liewehr B.; Kruse B.; Peltz C.; Witting T.; Husakou A.; Rouzee A.; Ivanov M.Y.; Fennel T.; Vrakking M.J.J.; Mermillod-Blondin A. Characterization of laser-induced ionization dynamics in solid dielectrics. *ACS Photonics* 2022, 9, 233–240. <https://doi.org/10.1021/acsp Photonics.1c01417>
13. Seuthe, T.; Mermillod-Blondin, A.; Grehn, M.; Bonse J.; Wondraczek L.; Eberstein M. Structural relaxation phenomena in silicate glasses modified by irradiation with femtosecond laser pulses. *Sci. Rep.* 7, 2017, 43815. <https://doi.org/10.1038/srep43815>
14. Bonse J.; Seuthe T.; Grehn M.; Eberstein M.; Rosenfeld A.; Mermillod-Blondin A. Time-resolved microscopy of fs-laser-induced heat flows in glasses. *Appl. Phys. A* 2018, 124, 60. <https://doi.org/10.1007/s00339-017-1465-5>
15. Meany, T.; Grafe, M.; Heilmann, R.; Perez-Leija, A.; Gross, S.; Steel, M.J.; Withford, M.J.; Szameit, A. Laser written circuits for quantum photonics. *Laser Photonics Rev.* 2015, 9, 363–384. <https://doi.org/10.1002/lpor.201500061>
16. Y. Nasu, M. Abe, M. Kohtoku, Developments in laser processing for silica-based planar lightwave circuits. *Proc. SPIE* 6107 (2006) 61070B. <https://doi.org/10.1117/12.647759>
17. Tan, D.; Zhang, B.; Qiu, J. Ultrafast Laser Direct Writing in Glass: Thermal Accumulation Engineering and Applications. *Laser Photonics Rev.* 15 (2021) 2000455. <https://doi.org/10.1002/lpor.202000455>
18. Lu, J.; Tian, J.; Poumellec, B.; Garcia-Caurel, E.; Ossikovski, R.; Zeng, X.; Lancry, M. Tailoring chiral optical properties by femtosecond laser direct writing in silica. *Light. Sci. Appl.* 2023, 12, 46. <https://doi.org/10.1038/s41377-023-01080-y>
19. Juodkazis, S.; Horyama, M.; Miwa, M.; Watanabe, M.; Marcinkevicius, A.; Mizeikis, V.; Matsuo, S.; Misawa, H. Stereolithography and 3D microstructuring of transparent materials by femtosecond laser irradiation. *Proc. SPIE*, 2002, 4644, 27-38. <https://doi.org/10.1117/12.464145>
20. Lencer, D.; Salinga, M.; Wuttig, M. Design Rules for Phase-Change Materials in Data Storage Applications. *Advanced Materials* 2011, 23, 2030-2058. <https://doi.org/10.1002/adma.201004255>
21. Hong, J.; Li, J.; Chu, D. Modulation approach of arbitrary linear polarization states of optical fields using single-beam coding for next-generation optical storage in glass. *Optics & Laser Technology* 2023, 164, 109539. <https://doi.org/10.1016/j.optlastec.2023.109539>
22. Lee, B.S.; Burr, G.W.; Shelby, R.M.; Raoux, S.; Rettner, C.T.; Bogle, S.N.; Darmawikarta, K.; Bishop, S.G.; Abelson, J.R. Observation of the role of subcritical nuclei in crystallization of a glassy solid. *Science* 2009, 326, 980-984. <https://doi.org/10.1126/science.1177483>
23. Wang, Z.; Tan, D.; Qiu, J. Single-shot photon recording for three-dimensional memory with prospects of high capacity. *Optics Letters* 2020, 45, 6274-6277. <https://doi.org/10.1364/OL.409171>
24. Huang, X.; Guo, Q.; Yang, D.; Xiao, X.; Liu, X.; Xia, Z.; Fan, F.; Qiu, J.; Dong, G. Reversible 3D laser printing of perovskite quantum dots inside a transparent medium. *Nature Photonics* 2020, 14, 82–88. <https://doi.org/10.1038/s41566-019-0538-8>
25. Li, X.; Wu, Y.; Lin, H.; Chen, G.; Hao, Y.; Wang, P.; Lin, S.; Xu, J.; Cheng, Y.; Wang, Y. Photochromic 3D Optical Storage: Laser-Induced Regulation of Localized Optical Basicity of Glass. *Laser Photonics Rev.* 2023, 2300744. <https://doi.org/10.1002/lpor.202300744>

26. Jin, M.; Zhou, W.; Ma, W.; Wang, Q.; Liang, X.; Zhang, P.; Xiang, W. The inhibition of CsPbBr₃ nanocrystals glass from self-crystallization with the assistance of ZnO modulation for rewritable data storage. *Chemical Engineering Journal* 2022, 427, 129812. <https://doi.org/10.1016/j.cej.2021.129812>
27. Sun, S.; Cheng, Z.; Song, J.; Yan, C.; Man, T.; Dong, G.; Qian, B.; Qiu, J. Low-Power-Consumption, Reversible 3D Optical Storage Based on Selectively Laser-Induced Photoluminescence Degradation in CsPbBr₃ Quantum Dots Doped Glass. *Adv. Mater. Technol.* 2022, 7, 2200470. <https://doi.org/10.1002/admt.202200470>
28. Wang, H.; Lei, Y.; Wang, L.; Sakakura, M.; Yu, Y.; Shayeganrad, G.; Kazansky, P.G. 100-Layer Error-Free 5D Optical Data Storage by Ultrafast Laser Nanostructuring in Glass. *Laser Photonics Rev.* 2022, 16, 2100563. <https://doi.org/10.1002/lpor.202100563>
29. Fedotov, S.; Lipatiev, A.; Lipateva, T.; Lotarev, S.; Melnikov, E.; Sigaev, V. Femtosecond laser-induced birefringent microdomains in sodium-borate glass for highly secure data storage. *J. American Ceramic Society* 2021, 104, 4297–4303. <https://doi.org/10.1111/jace.17868>
30. Su, Z.; Sun, S.; Dai, Y.; Liu, X.; Qiu, J. Femtosecond laser direct-writing of perovskite nanocrystals in glasses. *J. Non-Cryst. Solids: X* 2023, 18, 100182. <https://doi.org/10.1016/j.nocx.2023.100182>
31. Lu, J.; Tian, J.; Poumellec, B.; Garcia-Caurel, E.; Ossikovski, R.; Zeng, X.; Lancry, M. Tailoring chiral optical properties by femtosecond laser direct writing in silica. *Light Sci. Appl.* 2023, 12, 46. <https://doi.org/10.1038/s41377-023-01080-y>
32. Azkona, J.J.; Martinez-Calderon, M.; Granados, E.; Gomez-Aranzadi, M.; Rodriguez, A.; Olaizola, S.M. Femtosecond laser fabrication of volume-phase gratings in CdS_xSe_{1-x} doped borosilicate glass at a low repetition rate. *Appl. Opt.* 2019, 58, 4220 – 4226. <https://doi.org/10.1364/AO.58.004220>
33. Lotarev, S.V.; Fedotov, S.S.; Pomigueva, A.I.; Lipatiev, A.S.; Sigaev, V.N. Effect of Pulse Repetition Rate on Ultrafast Laser-Induced Modification of Sodium Germanate Glass. *Nanomaterials* 2023, 13, 1208. <https://doi.org/10.3390/nano13071208>
34. Vetchinnikov, M.P.; Lipatiev, A.S.; Shakhgildyan, G.Y.; Golubev, N.V.; Ignateva, E.S.; Fedotov, S.S.; Lipatieva, T.O.; Lotarev, S.V.; Vilkovisky, G.A.; Sigaev, V.N. Direct femtosecond laser-induced formation of CdS quantum dots inside silicate glass. *Optics Letters* 2018, 43, 2519-2522. <https://doi.org/10.1364/OL.43.002519>
35. Bera, D.; Qian, L.; Tseng, T.K.; Holloway, P.H. Quantum Dots and Their Multimodal Applications: A Review. *Materials* 2010, 3, 2260-2345. <https://doi.org/10.3390/ma3042260>
36. Lipatiev, A.S.; Shakhgildyan, G.Y.; Vetchinnikov, M.P.; Lotarev, S.V.; Lipatieva, T.O.; T.O. Sigaev, T.O. Laser writing of luminescent microdomains with CdS quantum dots in silicate glass. *Glass and Ceramics* 2021, 77, 369–371. <https://doi.org/10.1007/s10717-021-00309-9>
37. Korkut, C.; Cinar, K.; Kabacelik, I.; Turan, R.; Kulakci, M.; Bek, A. Laser Crystallization of Amorphous Ge Thin Films via a Nanosecond Pulsed Infrared Laser. *Crystal Growth & Design* 2021, 21, 4632-4639. <https://doi.org/10.1021/acs.cgd.1c00470>
38. Zhang, Y.; Liu, H.; Mo, J.; Wang, M.; Chen, Z.; He, Y.; Yang, W.; Tang, C. Atomic-level crystallization in selective laser melting fabricated Zr-based metallic glasses. *Phys. Chem. Chem. Phys.* 2019, 21, 12406-12413. <https://doi.org/10.1039/C9CP02181G>
39. Phillips, K.C.; Gandhi, H.H.; Mazur, E.; Sundaram, S.K. Ultrafast laser processing of materials: a review. *Adv. Opt. Photon.* 2015, 7, 684-712. <https://doi.org/10.1364/AOP.7.000684>
40. Tan, D.; Sharafudeen, K.N.; Yue, Y.; Qiu, J. Femtosecond laser induced phenomena in transparent solid materials: Fundamentals and applications. *Progress in Materials Science* 2016, 76, 154-228. <https://doi.org/10.1016/j.pmatsci.2015.09.002>
41. Ams, M.; Marshall, G.D.; Dekker, P.; Dubov, M.; Mezentsev, V.K.; Bennion, I.; Withford, M.J. Investigation of Ultrafast Laser-Photonic Material Interactions: Challenges for Directly Written Glass Photonics. *IEEE J. Selected Topics in Quantum Electronics* 2008, 14, 1370-1381. <https://doi.org/10.1109/JSTQE.2008.925809>
42. Gamaly, E.G.; Juodkasis, S.; Nishimura, K.; Misawa, H.; Luther-Davies, B.; Hallo, L.; Nicolai, P.; Tikhonchuk, V.T. Laser-matter interaction in the bulk of a transparent solid: Confined microexplosion and void formation. *Phys. Rev. B* 2006, 73, 214101. <https://doi.org/10.1103/PhysRevB.73.214101>
43. Schaffer, C.B.; Brodeur, A.; Mazur, E. Laser-induced breakdown and damage in bulk transparent materials induced by tightly focused femtosecond laser pulses. *Meas. Sci. Technol.* 2001, 12, 1784–1794. <https://doi.org/10.1088/0957-0233/12/11/3>
44. Lancry, M.; Regnier, E.; Poumellec, B. Fictive temperature in silica-based glasses and its application to optical fiber manufacturing. *Progress in Materials Science* 2012, 57, 63-94. <https://doi.org/10.1016/j.pmatsci.2011.05.002>
45. Debenedetti, P.; Stillinger, F. Supercooled liquids and the glass transition. *Nature* 2001, 410, 259–267. <https://doi.org/10.1038/35065704>
46. Yoshino, T.; Ozeki, Y.; Matsumoto, M.; Itoh, K. In situ Micro-Raman Investigation of Spatio-Temporal Evolution of Heat in Ultrafast Laser Microprocessing of Glass. *Japanese Journal of Applied Physics* 2012, 51, 102403. <https://doi.org/10.1143/JJAP.51.102403>

47. Richter, S.; Hashimoto, F.; Zimmermann, F.; Ozeki, Y.; Itoh, K.; Tunnermann, A.; Nolte, S. Spatial and temporal temperature distribution of ultrashort pulse induced heat accumulation in glass. *Proceedings Volume 9355, Frontiers in Ultrafast Optics: Biomedical, Scientific, and Industrial Applications XV*; 935515 (2015). <https://doi.org/10.1117/12.2078939>
48. Richter, S.; Zimmermann, F.; Tunnermann, A.; Nolte, S. Laser welding of glasses at high repetition rates – Fundamentals and prospects. *Optics & Laser Technology* 2016, 83, 59-66. <https://doi.org/10.1016/j.optlastec.2016.03.022>
49. Shakhgildyan, G.Y.; Lipatiev, A.S.; Vetchinnikov, M.P.; Popova, V.V.; Lotarev, S.V.; Golubev, N.V.; Ignateva, E.S.; Presniakov, M.M.; Sigaev, V.N. One-step micro-modification of optical properties in silver-doped zinc phosphate glasses by femtosecond direct laser writing. *J. Non-Cryst. Sol.* 2018, 481, 634-642. <https://doi.org/10.1016/j.jnoncrysol.2017.12.011>
50. Kunwar, P.; Soman, P. Direct Laser Writing of Fluorescent Silver Nanoclusters: A Review of Methods and Applications. *ACS Appl. Nano Mater.* 2020, 3, 7325-7342. <https://dx.doi.org/10.1021/acsnm.0c01339>
51. Varkentina, N.; Cardinal, T.; Morote, F.; Mounaix, P.; Andre, P.; Deshayes, Y.; Canioni, L. Examination of femtosecond laser matter interaction in multipulse regime for surface nanopatterning of vitreous substrates. *Optics Express* 2013, 21, 29090-29100. <https://doi.org/10.1364/OE.21.029090>
52. Chen, L.; Guo, C.; Pan, M.; Lai, C.; Wang, Y.; Liao, G.; Ma, Z.; Zhang, F.; Suriyaprakash, J.; Guo, L.; Akinoglu, E.M.; Li, Q.; Wu, L. Sub-40 nm nanogratings self-organized in PVP-based polymer composite film by photoexcitation and two sequent splitting under femtosecond laser irradiation. *Appl. Surf. Sci.* 2023, 609, 155395. <https://doi.org/10.1016/j.apsusc.2022.155395>
53. Shimizu, M.; Sakakura, M.; Ohnishi, M.; Shimotsuma, Y.; Nakaya, T.; Miura, K.; Hirao, K. Mechanism of heat-modification inside a glass after irradiation with high-repetition rate femtosecond laser pulses. *J. Appl. Phys.* 2010, 108, 073533. <https://doi.org/10.1063/1.3483238>
54. Sakakura, M.; Terazima, M. Initial temporal and spatial changes of the refractive index induced by focused femtosecond pulsed laser irradiation inside a glass. *Phys. Rev. B* 2005, 71, 024113. <https://doi.org/10.1103/PhysRevB.71.024113>
55. Shimotsuma, Y.; Sakakura, M.; Miura, K.; Qiu, J.; Kazansky, P.G.; Fujita, K.; Hirao, K. Application of femtosecond-laser induced nanostructures in optical memory. *J. Nanosci. Nanotechnol.* 2007, 7, 94-104. <https://pubmed.ncbi.nlm.nih.gov/17455477>
56. Macedo, G.N.B.M.; Sawamura, S.; Wondraczek, L. Lateral hardness and the scratch resistance of glasses in the Na₂O-CaO-SiO₂ system. *J. Non-Cryst. Sol.* 2018, 492, 94-101. <https://doi.org/10.1016/j.jnoncrysol.2018.04.022>
57. Gonzalez-Oliver, C.J.R.; James, P.F. Crystal nucleation and growth in a Crystal nucleation and growth in a Na₂O-2CaO-3SiO₂ glass. *J. Non-Crystal. Sol.* 1980, 38-39, 699-704. [https://doi.org/10.1016/0022-3093\(80\)90518-9](https://doi.org/10.1016/0022-3093(80)90518-9)
58. Huang, J.; Gupta, P.K. Temperature dependence of the isostructural heat capacity of a soda lime silicate glass. *J. Non-Crystal. Sol.* 1992, 139, 239-247. [https://doi.org/10.1016/S0022-3093\(05\)80831-2](https://doi.org/10.1016/S0022-3093(05)80831-2)
59. Liu, B.; Liu, Q.; Li, B.; Behrens, H.; Lange, R.A. Ultrasonic studies of alkali-rich hydrous silicate glasses: Elasticity, density, and implications for water dissolution mechanisms. *American Mineralogist* 2023, 108, 744-753. <https://doi.org/10.2138/am-2022-8451>
60. Wang, M.; Cheng, J.; Li, M.; He, F.; Deng, W. Viscosity and thermal expansion of soda-lime-silica glass doped with Gd₂O₃ and Y₂O₃. *Solid State Sciences* 2012, 14, 1233-1237. <https://doi.org/10.1016/j.solidstatesciences.2012.06.001>
61. Bouras, N.; Madjoubi, M.A.; Kolli, M.; Benterki, S.; Hamidouche, M. Thermal and mechanical characterization of borosilicate glass. *Physics Procedia* 2009, 2, 1135-1140. <https://doi.org/10.1016/j.phpro.2009.11.074>
62. Wereszczak, A.A.; Anderson Jr, C.E. Borofloat and Starphire Float Glasses: A Comparison. *Int. J. Appl. Glass Science* 2014, 5, 334-344. <https://doi.org/10.1111/ijag.12095>
63. George, J.L.; Sugawara, T.; Ohira, T.; Kruger, A.A.; Vienna, J.D. Heat capacity of complex aluminoborosilicate glasses. *Int. J. Appl. Glass Sci.* 2022, 13, 576-590. <https://doi.org/10.1111/ijag.16566>
64. Moynihan, C.T.; Easteal, A.J.; De Bolt, M.A.; Tucker, J. Dependence of the Fictive Temperature of Glass on Cooling Rate. *J. American Ceramic Soc.* 1976, 59, 12-16. <https://doi.org/10.1111/j.1151-2916.1976.tb09376.x>
65. Lide, D.R. *CRC Handbook of Chemistry and Physics*, 90th ed.; CRC Press: Boca Raton, FL, USA, 2009; ISBN 13: 978-1420090840 / 10:1420090844
66. Birge, N.O.; Nagel, S.R. Specific heat spectroscopy of the glass transition. *Phys. Rev. Lett.* 1985, 54, 2674-2677. <https://doi.org/10.1103/PhysRevLett.54.2674>
67. Korus, J.; Beiner, M.; Busse, K.; Kahle, S.; Unger, R.; Donth, E. Heat capacity spectroscopy at the glass transition in polymers. *Thermochim. Acta* 1997, 304-305, 99-110. [https://doi.org/10.1016/S0040-6031\(97\)00028-2](https://doi.org/10.1016/S0040-6031(97)00028-2)

68. Chua, Y.Z.; Schulz, G.; Shoifet, E.; Huth, H.; Zorn, R.; Scmelzer, J.W.P.; Schick, C. Glass transition cooperativity from broad band heat capacity spectroscopy. *Colloid Polym. Sci.* 2014, 292, 1893-1904. <https://doi.org/10.1007/s00396-014-3280-2>
69. Minakov, A.; Schick, C. Nanometer scale thermal response of polymers to fast thermal perturbations. *J. Chem. Phys.* 2018, 149, 074503. <https://doi.org/10.1063/1.5044187>
70. Minakov, A.; Schick, C. Integro-Differential Equation for the Non-Equilibrium Thermal Response of Glass-Forming Materials: Analytical Solutions. *Symmetry* 2021, 13, 256. <https://doi.org/10.3390/sym13020256>
71. Minakov, A.; Schick, C. Thermal Perturbations at Crystal Nucleation in Glass-Forming Liquids. *Energies*, 2022, 15, 9005. <https://doi.org/10.3390/en15239005>
72. Minakov, A.A.; Schick, C. Nanoscale Heat Conduction in CNT-polymer Nanocomposites at Fast Thermal Perturbations. *Molecules* 2019, 24, 2794. <https://doi.org/10.3390/molecules24152794>
73. Landau, L.D.; Lifshitz, E.M. Course of Theoretical Physics 5: Statistical physics Part 1, 3rd ed., Pergamon press, Oxford, 1980. ISBN-10: 0750633727 / ISBN-13: 978-0750633727
74. Landau, L.D.; Lifshitz, E.M. Course of Theoretical Physics 8: Electrodynamics of Continuous Media, Butterworth-Heinemann, Oxford, 2nd ed., 2000. ISBN-10: 0750626348 / ISBN-13: 978-0750626347
75. Schilling, R.L.; Song, R.; Vondracek, Z. Bernstein Functions: Theory and Applications, Hubert & Co Berlin 2010. ISBN 978-3-11-021530-4, <https://doi.org/10.1515/9783110215311>
76. Johnston, D.C. Stretched exponential relaxation arising from a continuous sum of exponential decays. *Phys. Rev. B* 2006, 74, 184430. <https://doi.org/10.1103/PhysRevB.74.184430>
77. Berberan-Santos, M.N.; Bodunov, E.N.; Valeur, B. Mathematical functions for the analysis of luminescence decays with underlying distributions 1: Kohlrausch decay function (stretched exponential). *Chem. Phys.* 2005, 315, 171–182. <https://doi.org/10.1016/j.chemphys.2005.04.006>
78. Gupta, P.K.; Moynihan, C.T. Prigogine-Defay ratio for systems with more than one order parameter. *J. Chem. Phys.* 1976, 65, 4136-4140. <https://doi.org/10.1063/1.432870>
79. Sukenaga, S.; Endo, T.; Nishi, T.; Yamada, H.; Ohara, K.; Wakihara, T.; Inoue, K.; Kawanishi, S.; Ohta, H.; Shibata, H. Thermal Conductivity of Sodium Silicate Glasses and Melts: Contribution of Diffusive and Propagative Vibration Modes. *Front. Mater.* 2021, 8, 753746. <https://doi.org/10.3389/fmats.2021.753746>
80. Kim, Y.; Morita, K. Thermal Conductivity of Molten B₂O₃, B₂O₃-SiO₂, Na₂O-B₂O₃, and Na₂O-SiO₂ Systems. *J. Am. Ceram. Soc.* 2015, 98, 1588–1595. <https://doi.org/10.1111/jace.13490>
81. Shimizu, M.; Sakakura, M.; Ohnishi, M.; Yamaji, M.; Shimotsuma, Y.; Hirao, K.; Miura, K. Three-dimensional temperature distribution and modification mechanism in glass during ultrafast laser irradiation at high repetition rates. *Optics Express* 2012, 20, 934-940. <https://doi.org/10.1364/OE.20.000934>
82. Sakakura, M.; Terazima, M.; Shimotsuma, Y.; Miura, K.; Hirao, K. Heating and rapid cooling of bulk glass after photoexcitation by a focused femtosecond laser pulse. *Opt. Express* 2007, 15, 16800–16807. <https://doi.org/10.1364/OE.15.016800>
83. Vladimirov, V.S. A Collection of Problems on the Equations of Mathematical Physics. Springer Berlin, Heidelberg, 1986. ISBN 978-3-662-05560-1; <https://doi.org/10.1007/978-3-662-05558-8>
84. Schawe, J.E.K.; Hess, K.U. The kinetics of the glass transition of silicate glass measured by fast scanning calorimetry. *Thermochim. Acta* 2019, 677, 85-90. <https://doi.org/10.1016/j.tca.2019.01.001>
85. Li, Y.Z.; Zhao, L.Z.; Sun, Y.T.; Wen, P.; Bai, H.Y.; Wang, W.H. Effect of dynamical heterogeneity on heat capacity at glass transition in typical silicate glasses. *J. Appl. Phys.* 2015, 118, 244905. <https://doi.org/10.1063/1.4939074>

Disclaimer/Publisher's Note: The statements, opinions and data contained in all publications are solely those of the individual author(s) and contributor(s) and not of MDPI and/or the editor(s). MDPI and/or the editor(s) disclaim responsibility for any injury to people or property resulting from any ideas, methods, instructions or products referred to in the content.